Measurement 207 (2023) 112425

Contents lists available at ScienceDirect

Measurement

journal homepage: www.elsevier.com/locate/measurement

Powerline interference suppression of a textile-insulated capacitive biomedical sensor using digital filters

Charn Loong Ng [a,b], Mamun Bin Ibne Reaz [a,*], Sawal Hamid Bin Md Ali [a], Maria Liz Crespo [b], Andres Cicuttin [b], Muhammad Enamul Hoque Chowdhury [c,*], Serkan Kiranyaz [c], Noorfazila Binti Kamal [a]

[a] Centre of Advanced Electronic and Communication Engineering, Department of Electrical, Electronic and Systems Engineering, Universiti Kebangsaan Malaysia, 43600 Bangi, Selangor Darul Ehsan, Malaysia
[b] Multidisciplinary Laboratory, International Centre for Theoretical Physics (ICTP), Via Beirut, 31, 34151 Trieste, Italy
[c] Department of Electrical Engineering, Qatar University, Doha 2713, Qatar

ARTICLE INFO

Keywords:
Capacitive biomedical sensor
Textile
Digital notch filter
Digital comb filter
Wavelet denoise
Adaptive filter

ABSTRACT

This research evaluated a textile-insulated capacitive (TEX-C) biomedical sensor insulated by six types of textile materials namely cotton, linen, rayon, nylon, polyester, and PVC-textile. Each textile material creates a unique skin-electrode capacitance and affected the susceptibility of the TEX-C biomedical sensor towards the 50 Hz powerline interference (PLI) and its harmonics. Designing versatile TEX-C biosensor hardware that can tolerate different textile insulators while maintaining an optimum signal measurement quality proves to be a significant challenge. Five digital filters such as notch filter, comb filter, discrete wavelet transform, undecimated wavelet transform, and normalized least mean squares adaptive filter were implemented to compare their performance in suppressing the 50 Hz PLI and its harmonics. The comb filter yielded the best results in suppressing the 50 Hz PLI and its harmonics below −130 dB while improving the correlation coefficient of the EMG signals measured by TEX-C biomedical sensors and the wet contact electrode.

1. Introduction

Over the years, medical treatment and healthcare systems underwent a great revolution from a complex and costly machine to a compact and affordable personalize device [1–3]. The wearable sensing system is one of the emerging technologies that embed electronic systems into the garment to provide long-term personal health monitoring capability without geographical boundaries [4,5]. LifeGuard [6], WEALTHY [7], MagIC [8], Lifeshirt [9], Delsys Trigno System [10–12], and BTS Bioengineering FREEEMG® [13] are good examples of a wearable sensing system that allow the user to keep track of their daily physical activities and health condition. The capacitive biomedical sensor is one of the preferred sensing technologies for smart garment and wearable sensor applications because it is capable of capturing electrophysiological signals without direct electrical contact with the human body. It operates based on capacitive coupling methodology which allows a thin layer of an insulator such as a textile to be placed between the body and biomedical sensor [14–16]. This characteristic allows the capacitive biomedical sensor to seamlessly integrate with our daily outfits. Nevertheless, a capacitive biomedical sensor has a high input impedance in nature because of the electrically contactless characteristic between the biomedical sensor and the human body. Therefore, a capacitive biomedical sensor is highly susceptible to the 50 Hz/60 Hz powerline interference (PLI) in our surroundings [17–19]. The textile insulator placed between the biomedical sensor and the human body is one of the controlling factors that affect the amplitude of the PLI couple in the electrophysiological signal measurement results. The unique physical characteristics such as relative permittivity, thickness, and porosity of each textile material will alter the total input impedance of a capacitive biomedical sensor.

Several research groups designed and characterized textile-insulated capacitive (TEX-C) biomedical sensors for different applications. Ueno et al. (2007) explored using capacitive sensing methodology to measure electrocardiography (ECG) signals from the dorsal surface of the body [20]. The ECG electrode is insulated with a cotton bedsheet with different thicknesses and coupling pressure. Two 50 Hz analog notch

* Corresponding authors.
E-mail addresses: mamun@ukm.edu.my (M. Bin Ibne Reaz), mchowdhury@qu.edu.qa (M.E. Hoque Chowdhury).

https://doi.org/10.1016/j.measurement.2022.112425
Received 14 July 2022; Received in revised form 16 November 2022; Accepted 30 December 2022
Available online 2 January 2023

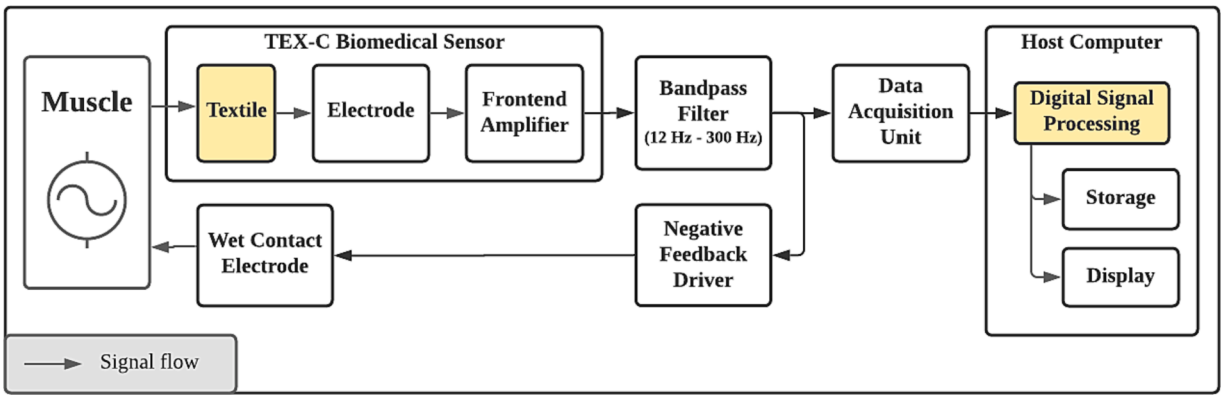

Fig. 1. The block diagram of a capacitive EMG monitoring system with a TEX-C biomedical sensor.

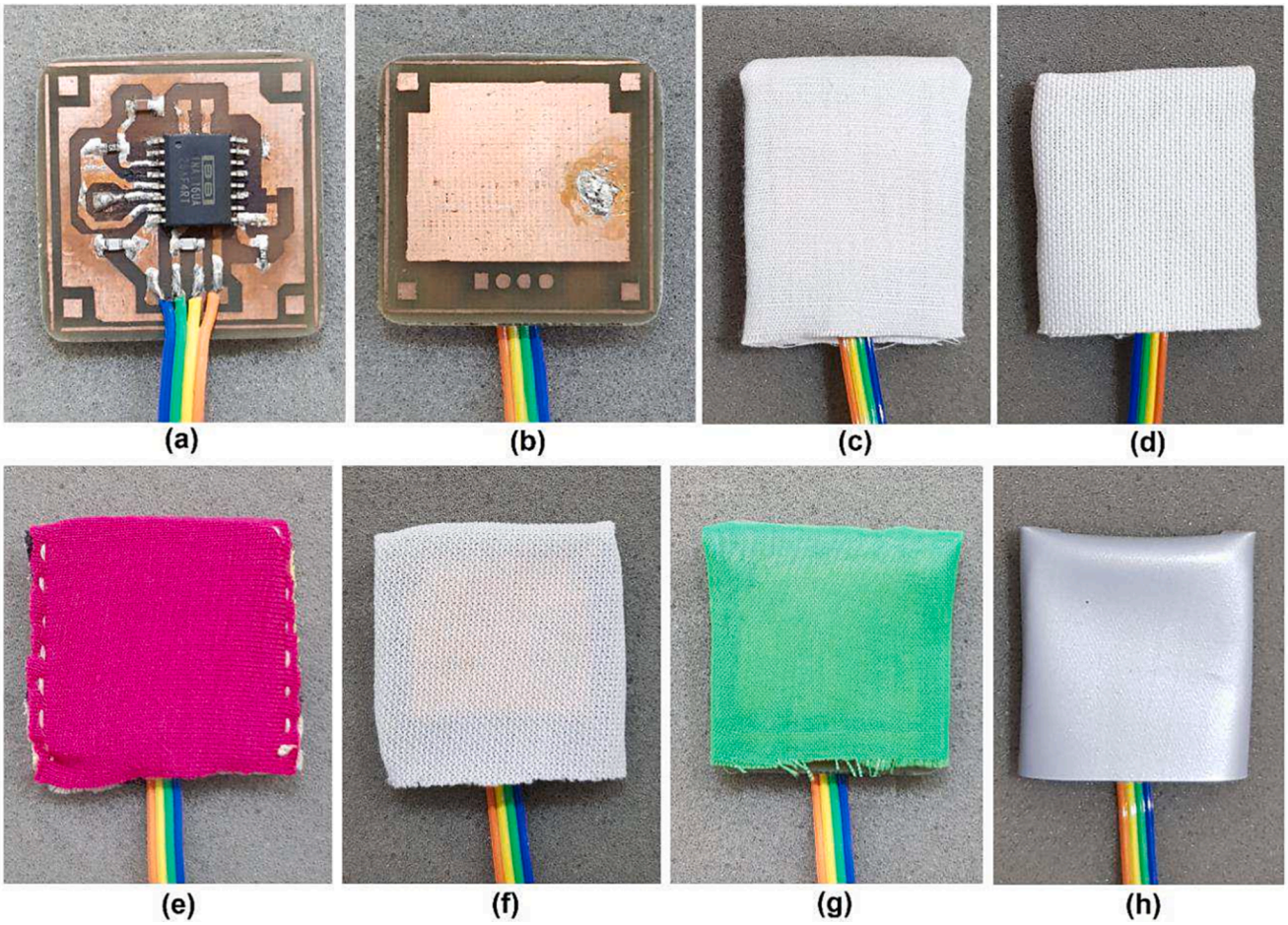

Fig. 2. The top view (a) and bottom view (b) of a TEX-C biomedical sensor without an insulator. Bottom view of TEX-C biomedical sensors insulated by (c) cotton, (d) linen, (e) rayon, (f) nylon, (g) polyester, and (h) PVC-textile.

filters were applied to remove the PLI and a 20-points moving average was implemented to suppress the noise. The experimental result shows that different levels of noise amplitude will still be coupled into the measurement results as the cotton bedsheet's thickness and coupling pressure varies. Li et al. (2015) also investigated the viability of a textile-based capacitive ECG acquisition system [21]. The capacitive ECG acquisition system has been designed with a 50 Hz analog notch filter by default. Cotton *T*-shirts with a thickness of 1.25 mm, 0.51 mm, and 0.78 mm were used as an insulator of the capacitive ECG sensor. The experimental results show that the thicker the cotton *T*-shirt, the lower the quality of the ECG signals collected, which were affected by noise. Hou et al. (2018) proposed to capture ECG signals using multiple unipolar capacitive electrodes, in which the subject is wearing an uneven thickness of clothes [22]. The system was designed with a 50 Hz analog notch filter and a 50 Hz digital notch filter to suppress the PLI. Pfeiffer et al. (2019) analyzed the effect of contact imbalance on a capacitive biomedical sensor caused by motion during ECG measurement [23]. Different types of capacitive electrodes such as copper plate electrode, conductive foam, moss embroidered electrode, and conductive fabric electrode were tested in the experiment. The result shows that different types of electrodes will create different levels of impedance imbalance during a dynamic muscle movement and eventually affect the level of

Table 1
Skin-electrode capacitance of TEX-C biomedical sensors. [25].

TEX-C biomedical sensor	Relative Permittivity, ε_r	Textile thickness (mm), d	Skin-electrode capacitance (pF), C_s
Cotton	3.004	0.23	58.96
Linen	4.007	0.40	45.22
Rayon	5.082	0.58	39.56
Nylon	1.222	0.48	11.49
Polyester	1.178	0.16	33.24
PVC-Textile	3.118	0.24	58.65

Table 2
Filter coefficients and configuration parameters of the IIR digital notch filter.

Filter Coefficients & Configuration Parameters	Values
Filter type	Notch Filter
Center frequency, f_0 (Hz)	50 Hz
Q-factor	20
Sampling frequency, f_s (Hz)	600
a_0	−1.70967
a_1	0.974157
b_0	0.987078
b_1	−1.70967

PLI coupled to the electrophysiological signal measurement result. Takano et al. (2021) explored using a capacitive cloth electrode to measure ECG and electromyography (EMG) from the neck [24]. The insulating textile is 100 % polyester with a thickness of 0.45 μm. The developed capacitive cloth electrodes consist of two 50 Hz analog notch filters, each for ECG and EMG signal paths. The measurement result shows that EMG burst signals can be captured when the subject coughs. However, the noise floor was high while the EMG signals were weak, therefore the signal-to-noise ratio of the measurement results was low.

In summary, most of the research groups were focusing on the cotton-insulated capacitive biomedical sensor, leaving a wide range of textile materials unexplored. The physical characteristics of a textile

Table 3
Configuration parameters and values of the IIR digital comb filter.

Filter Coefficients & Configuration Parameters	Values
Filter type	Comb filter - Notch Type I
Center frequency, f_0 (Hz)	50 Hz
Define full bandwidth, Df (Hz)	0.02
Sampling frequency, f_s (Hz)	600
a	0.668487
b	0.834243
N	12

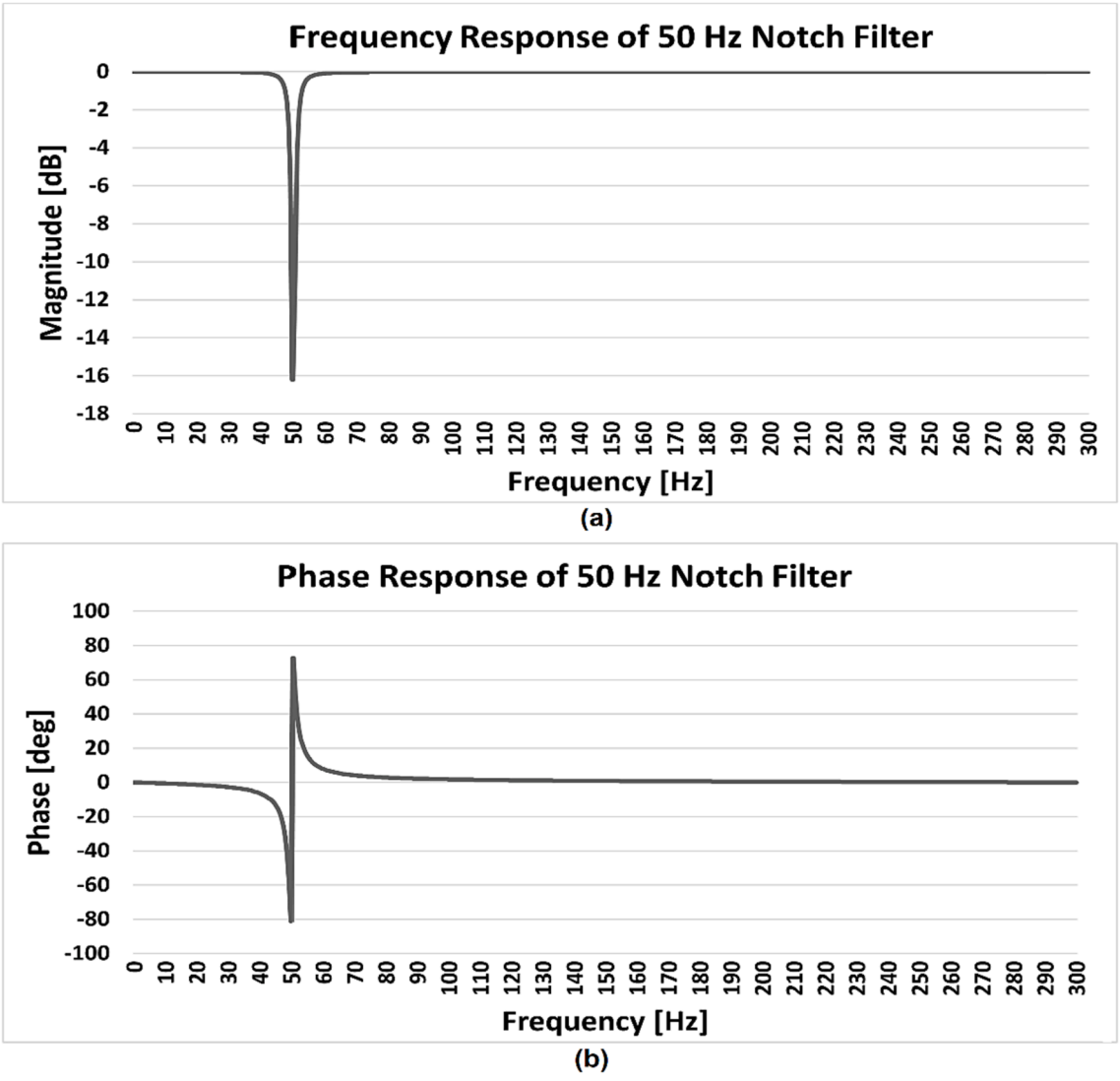

Fig. 3. Frequency response and phase response of the 50 Hz digital notch filter.

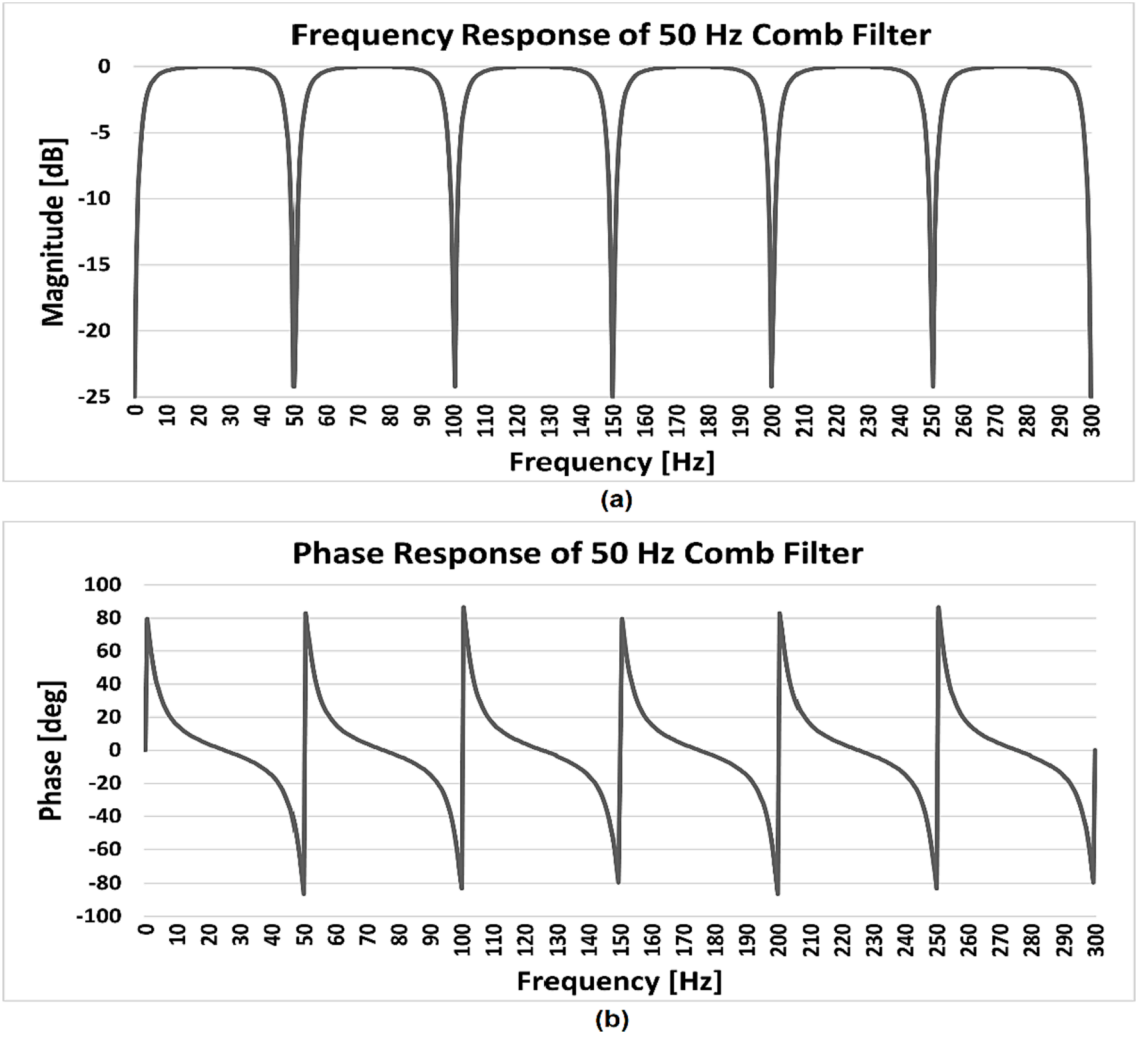

Fig. 4. Frequency response and phase response of the 50 Hz digital comb filter.

Table 4
Configuration parameters and values of the discrete wavelet transform.

Parameters	Values
Transform type	Discrete Wavelet Transform (DWT)
Wavelet	Daubechies, db14
Level	3
Thresholding rule	Universal
Rescaling method	Single level

Table 5
Configuration parameters and values of the undecimated wavelet transform.

Parameters	Values
Transform type	Undecimated Wavelet Transform (UWT)
Wavelet	Daubechies, db14
Level	3
Thresholding rule	Universal
Rescaling method	Single level

insulator were proven to alter the noise floor and performance of a TEX-C biomedical sensor [20,21,25]. The PLI was acknowledged as one of the main signal interferences while most of the research groups were relying on an analog notch filter to attenuate the PLI [26]. However, designing an analog filter on board will increase the overall biomedical sensor size. Regardless of Twin-T analog notch filter, Fliege analog notch filter, or integrated circuit, they all require high-precision passive components to achieve an accurate center frequency, and a high Q-factor remains a circuit design challenge [21,27]. The goal of this paper is to propose a simplified system architecture that allows the generic hardware of TEX-C biomedical sensors to yield a quality EMG signal measurement without constraint by the types of textile insulators. The methodologies are: (1) Characterize the PLI on six TEX-C biomedical sensors insulated by cotton, linen, rayon, nylon, polyester, and PVC-textile. These textile samples are the most common materials used in daily garment production. (2) Evaluate the effectiveness of five types of digital filters in suppressing the PLI across the six different types of TEX-C biomedical sensors. The experiment evaluates the TEX-C biomedical sensors baseline characterization, EMG burst signals measurement quality, and performance correlation with the gold standard, wet contact electrode [28,29]. The performances of these digital filters were compared, and the most versatile solution was proposed based on the effectiveness of PLI suppression across six types of TEX-C biomedical sensors [28,29].

2. Methods and materials

2.1. Electromyography acquisition and pre-processing modules

The architecture and electrical circuitry of a capacitive EMG monitoring system were described in detail by Ng et al. (2020) [30]. The system consists of TEX-C biomedical sensors, frontend amplifiers,

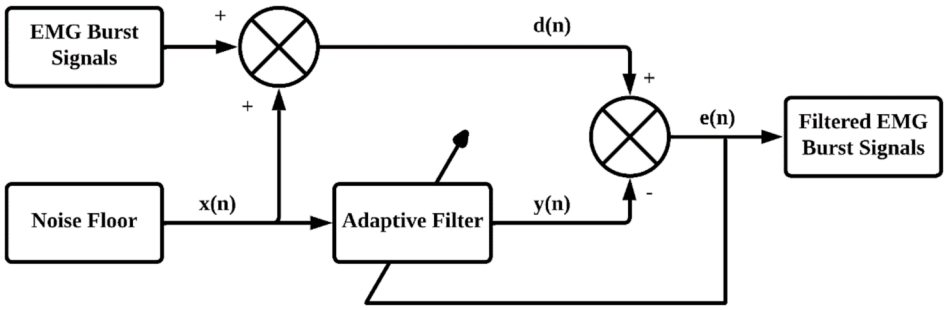

Fig. 5. Block diagram of the NLMS adaptive filter.

Table 6
Configuration parameters and values of the NLMS adaptive filter.

Input Parameters	Values
Filter type	FIR NLMS
Polymorphic instance	Real
Filter length	6000 (10 s)
Step Size	0.1
Leaky factor	0

bandpass filter, data acquisition unit, host computer, and negative feedback driver as shown in Fig. 1. The arrows in Fig. 1 indicate the flow direction of the EMG signals. The bandpass filter in the system is an anti-aliasing filter that limits the input frequency bandwidth of the EMG monitoring system between 12 Hz and 300 Hz. This passband frequency range is set to target the dominant frequency range of EMG signals [16,31]. Since the 50 Hz or 60 Hz PLI also falls within the passband frequency range, hence the PLI is expected to couple into the EMG measurement results. The digital signal processing stage mainly contains five different digital filters which are presented in Section 2.3. The effectiveness of these digital filters to suppress the 50 Hz PLI and its harmonics were evaluated with experimental data.

Fig. 2(a) and 2(b) exhibit the top and bottom views of a capacitive biomedical sensor without a textile insulator. The capacitive biomedical sensor was designed on a rigid printed circuit board (PCB). The top layer consists of a frontend amplifier circuitry while the bottom layer is a capacitive coupling electrode made of a copper plate. The capacitive biomedical sensors insulated by cotton, linen, rayon, nylon, polyester, and PVC-textile are shown in Fig. 2(c)–2(h) [25].The capacitance

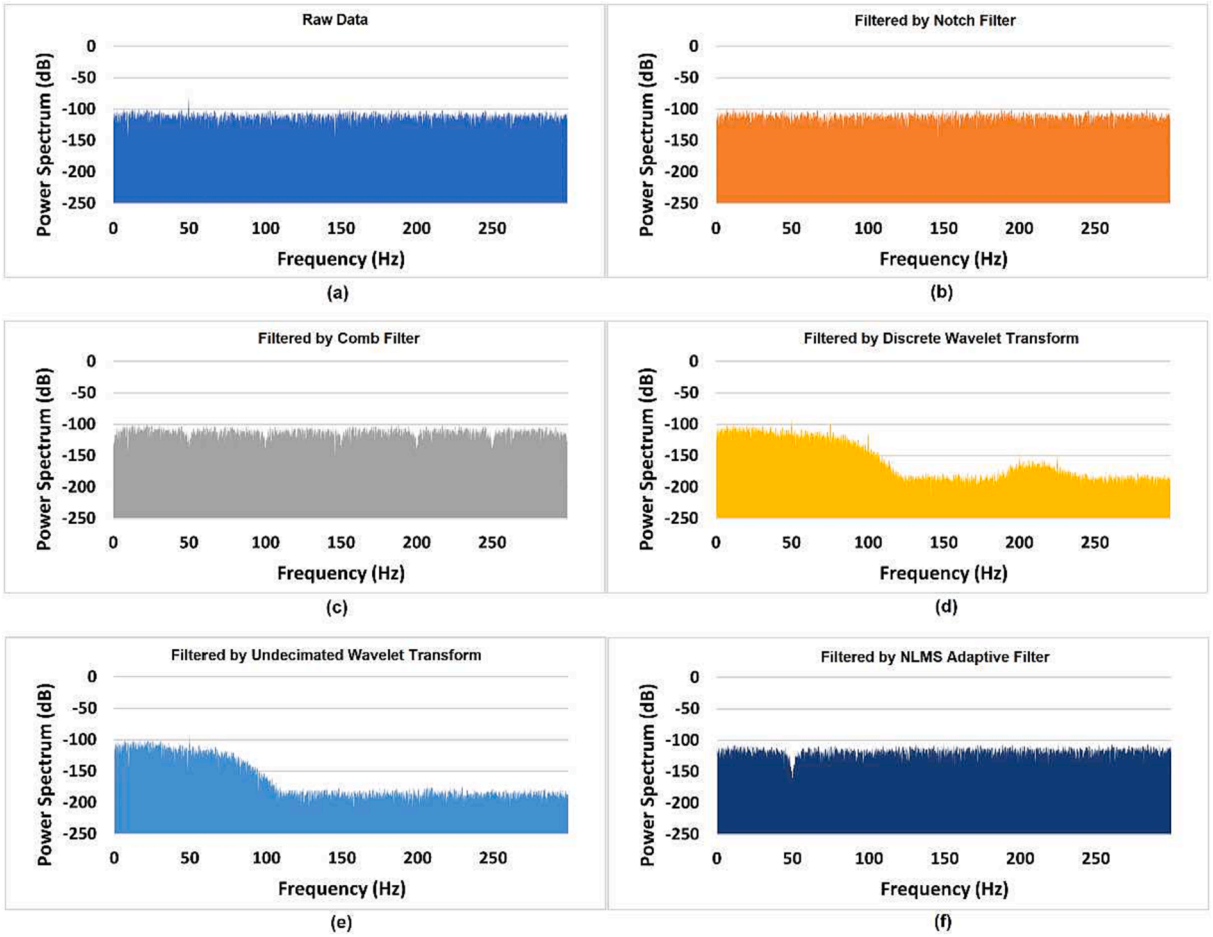

Fig. 6. Spectrum analysis of baseline data recorded by cotton TEX-C biomedical sensor.

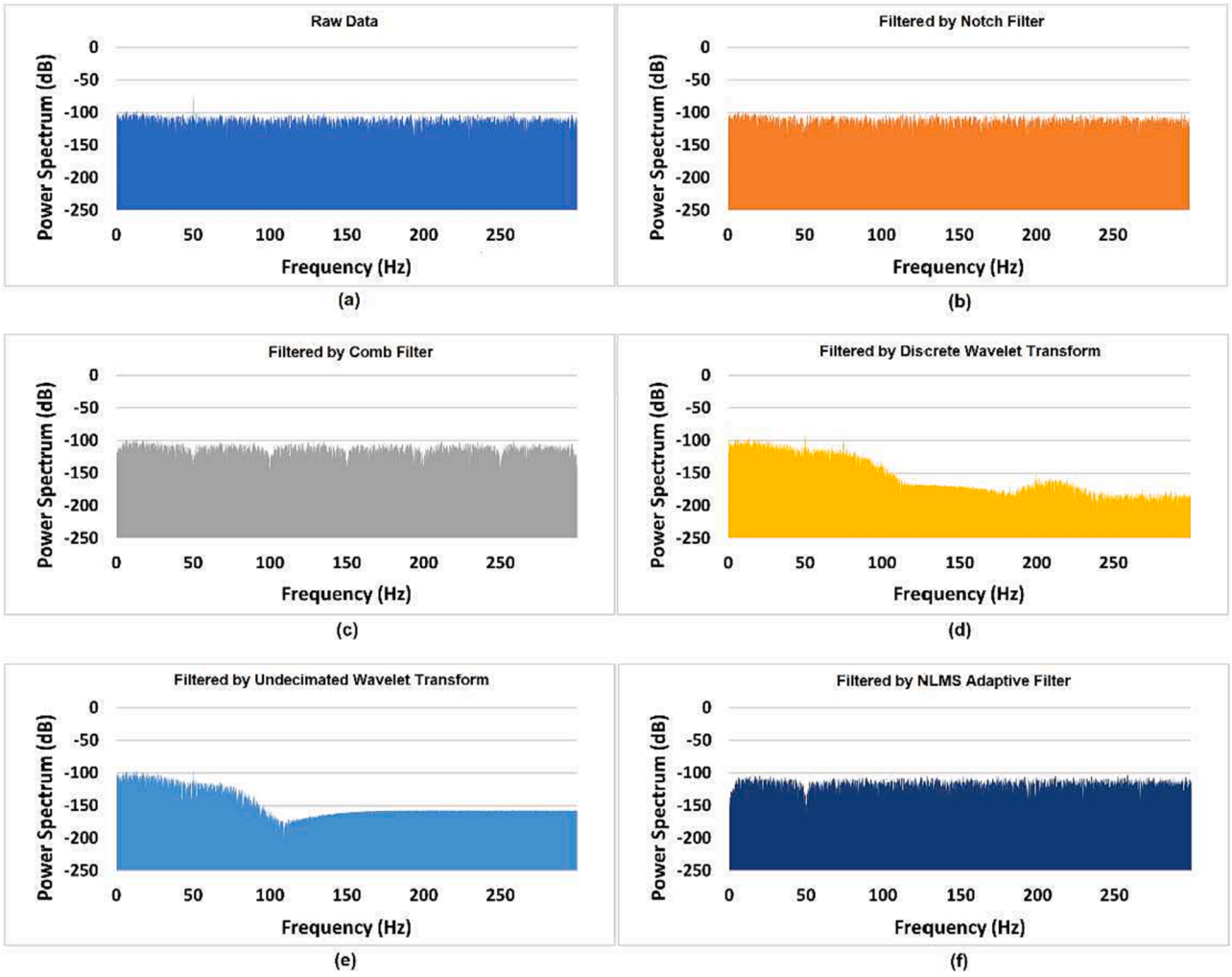

Fig. 7. Spectrum analysis of baseline data recorded by linen TEX-C biomedical sensor.

created between the sensor electrode and the body is called skin-electrode capacitance. The skin-electrode capacitance can be derived using a parallel plate capacitor model, for example using the equation (1). The skin-electrode capacitance is controlled by parameters such as textile material, the area size of the sensing metal plate, and the distance between the biomedical sensor and the body. The skin-electrode capacitance values of all the TEX-C biomedical sensors are presented in Table 1.

$$C_s = \frac{\varepsilon_r \varepsilon_o A}{d} \tag{1}$$

where

C_s is the skin-electrode capacitance of the TEX-C biomedical sensor;
ε_0 is the permittivity of free space with the value of $8.854 \times 10^{-12} F/m$;
ε_r is the dielectric constant of textile material;
A is the metal plate area size of a TEX-C biomedical sensor, 510 mm^2;
d is the distance between the TEX-C biomedical sensor metal plate and body.

These six textiles were chosen because they are common materials to make our daily outfit, sportswear, muscle relief and support band. Cotton and linen are natural textile which made from cotton plant and flax plant [32,33]. Both textiles are hypoallergenic and breathable. Rayon, nylon, polyester, and PVC-textile are synthetic textiles which made of regenerative cellulose and polymer [34,35]. These textile materials were created or their unique advantages such as elasticity, strong abrasion resistance, and water resistance. It is worth to take note that the process of creating synthetic fiber typically involves chemicals, dyes, and bleaching agents. They might not be a suitable for users with sensitive skin. Table 1 presents the initial properties of each textile material that were used in the experiment. For a long-term application, the processes of washing, drying, and material degradation tend to change these properties. Since these secondary effects were not the focus of this research, thus their impacts were not included in this paper.

2.2. Powerline interference and harmonics

The powerline interference originates from the alternating current (AC) of the power grid which typically switches at the fundamental frequency of 50 Hz or 60 Hz. When a non-linear load is connected to the power grid to draw current, it will generate the harmonic frequencies on top of the fundamental frequency [36]. The 50 Hz or 60 Hz PLI and their harmonic frequencies are commonly present in our surroundings of power supply cords and electrical appliances. PLI can affect the sensor's measurement result through resistive contact, inductive coupling, and capacitive coupling method. The total voltage of PLI, V_{pli} is represented by Equation (2) and Equation (3) [21,25]. Equation (4) shows the relationship between the amplitude of the PLI in the electrophysiological signal measurement and the physical characteristics of a textile insulator [37].

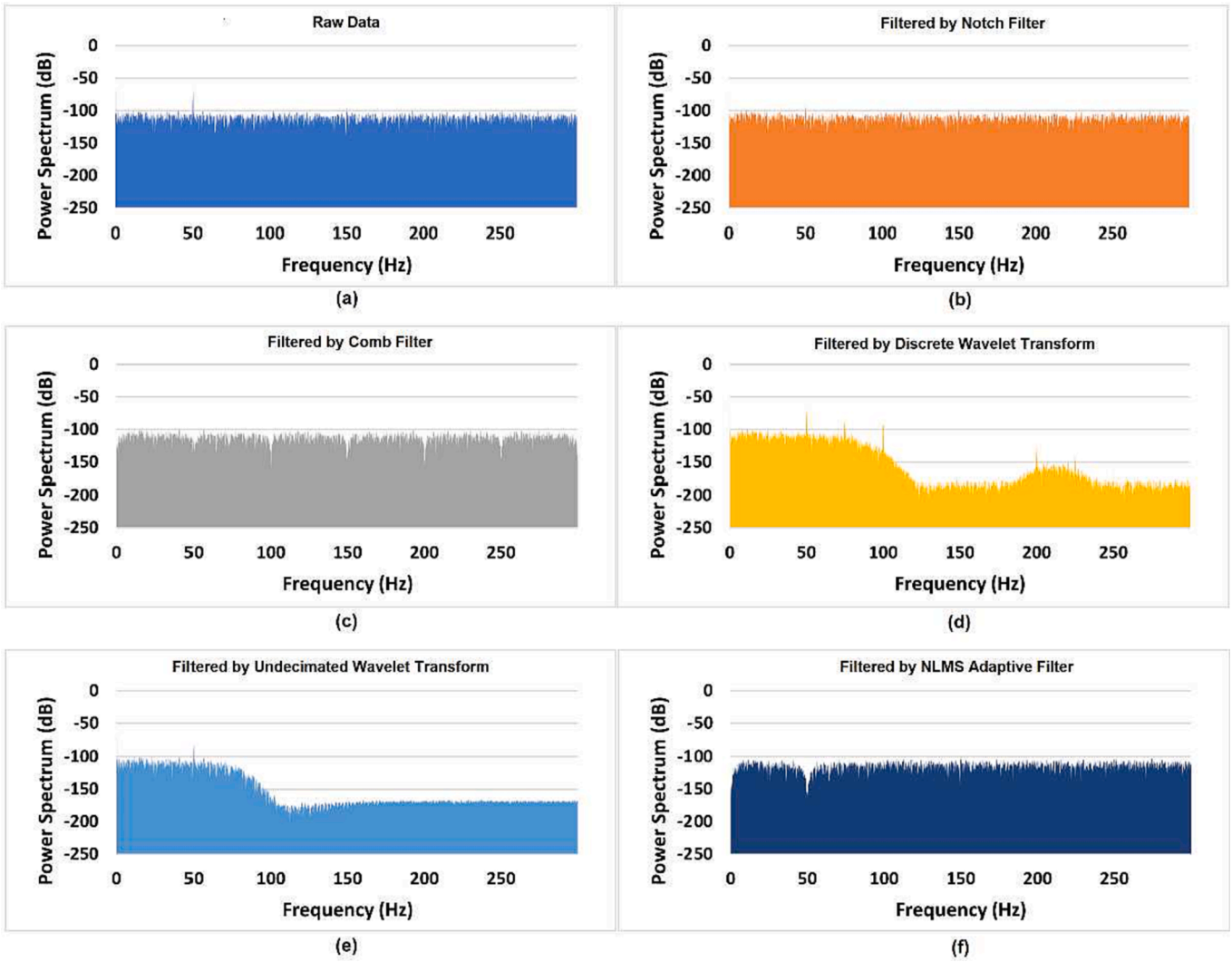

Fig. 8. Spectrum analysis of baseline data recorded by rayon TEX-C biomedical sensor.

$$V_{pli} = V_{pli-R} + V_{pli-L} + V_{pli-C} \tag{2}$$

$$V_{pli} = I_R R + I_L(j\omega L) + I_{cm}\left(\frac{1}{j\omega C_s}\right) \tag{3}$$

$$V_{pli} = I_R R + I_L(j\omega)\left(\frac{\mu N^2 A_L}{l}\right) + I_{cm}\left(\frac{1}{j\omega}\right)\left(\frac{d}{\varepsilon_r \varepsilon_o A}\right) \tag{4}$$

where

V_{pli} is the total voltage amplitude of the powerline interference;
V_{pli-R} is the powerline interference voltage source from resistive contact;
V_{pli-L} Is the powerline interference voltage source from induction;
V_{pli-C} is the powerline interference voltage source from capacitive coupling;
I_R is the direct conductive current between the sensor and powerline interference;
R is the resistance along the conductive path between the sensor and powerline;
I_L is the current induced to the conductive path between the electrode and frontend amplifier;
L is inductance in Henry (H);
I_{cm} is the induced common mode current;
μ is the permeability of the core material;
N is the number of turns of a coil;
A_L is the area size circled by coil (m^2);
l is the length of coil (m);

Since the TEX-C biomedical sensors measure the electrophysiological signals through capacitive coupling methodology, the sensor's electrode is contactless to the human body and other electrical devices. Thus, the V_{pli-R} contributed through resistive contact is expected to be 0 V. The sensor's electrode is a flat copper plate as shown in Fig. 2b with a short copper trace connected to the frontend amplifier on the topside of the rigid PCB. Thus, the V_{pli-L} contributed through magnetic field induction to the sensor's metal plate is negligible. The V_{pli-C} is expected to be the dominant source of V_{pli} because TEX-C biomedical sensor is designed with an insulated metal electrode connected to a frontend buffer with high input impedance characteristic. Equation (3) shows that the skin-electrode capacitance, C_s and the V_{pli} are inversely proportional. The higher the skin-electrode capacitance, the lower the PLI voltage coupled to the measurement results [38]. Equation (4) is aligned with the previous research group findings where the unique physical properties of each textile material such as thickness, porosity, and relative permittivity will affect the amplitude of the PLI coupled to the electrophysiological signal measurement.

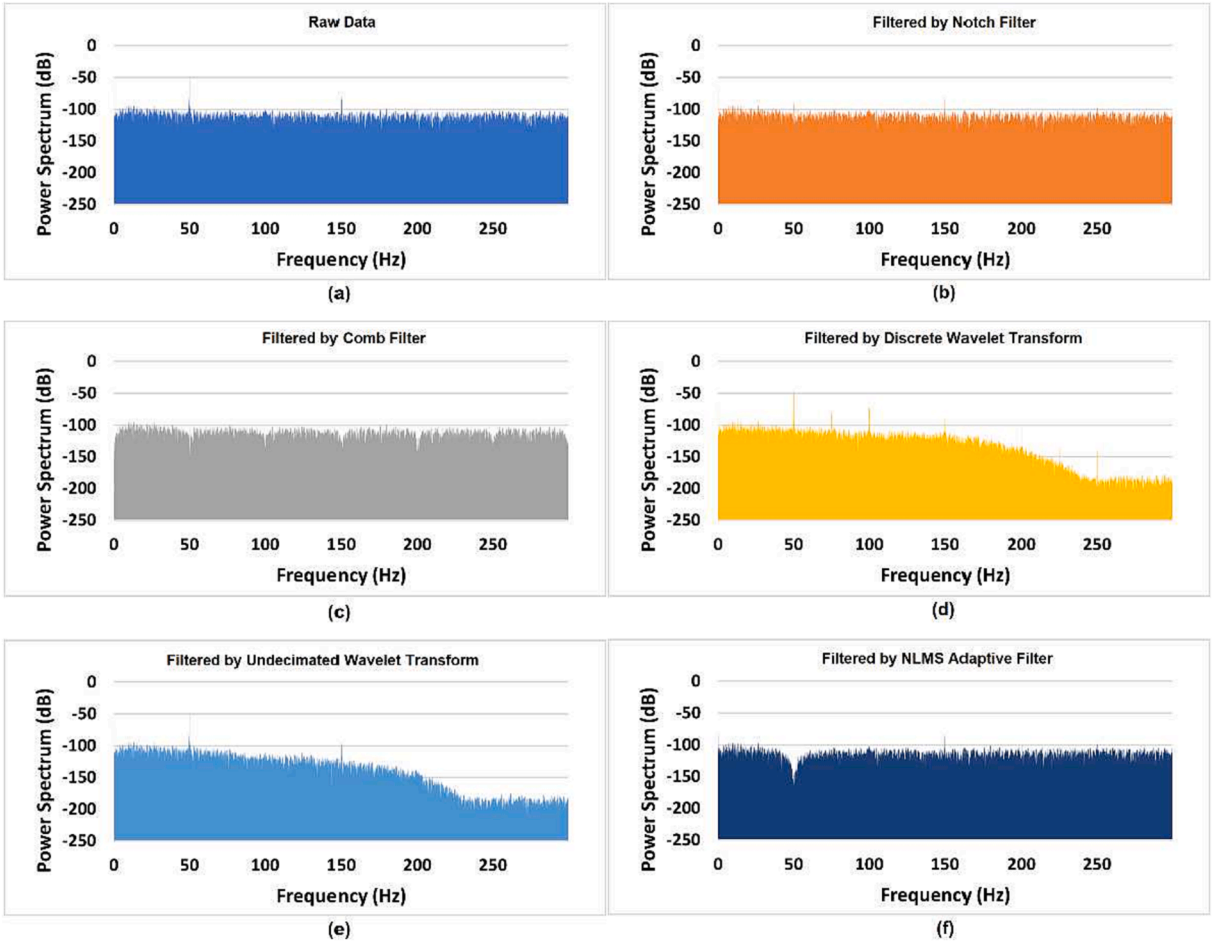

Fig. 9. Spectrum analysis of baseline data recorded by nylon TEX-C biomedical sensor.

2.3. Digital signal processing

A digital filter is a common digital signal processing technique, use to suppress or eliminate unwanted components in digitized data. There are a total of five digital filters being explored in this research which are digital notch filter, digital comb filter, discrete wavelet transform (DWT), undecimated wavelet transform (UWT), and normalized least mean squares (NLMS) adaptive filter. Daniel et al.'s (2018) literature review corroborates that these digital filters were proposed and implemented by various researchers to suppress the PLI in electrophysiological signal measurement applications [36]. All the digital filters were designed with LabVIEW Digital Filter Design (DFD) Toolkit and implemented in the real-time data acquisition. The fundamental frequency of the PLI in the experimental environment is 50 Hz. So, all the digital filters were designed based on this targeted PLI frequency.

2.3.1. Digital notch filter

The notch filter is a common technique to suppress the PLI as reviewed in Section 1. A digital notch filter provides more flexibility to configure the coefficient compared to an analog notch filter [39–42]. The design methodology of this notch filter is based on the window method. The LabVIEW DFD IIR Notch Peak Design VI by Q factor is selected because the targeted band-stop frequency is at 50 Hz. Since the dominant EMG signals frequency is range between 12 Hz and 300 Hz, the Q factor of 20 is selected to achieve a sharp filter notch at 50 Hz while maintaining a constant gain across the remaining passband frequency. Then, the filter coefficients are generated accordingly. All the design parameters of an infinite impulse response (IIR) digital notch filter were listed in Table 2. Equation (5) shows the transfer function of the IIR digital notch filter. Fig. 3 shows the relation of the frequency response and phase response graphs of the 50 Hz digital notch filter.

$$H(z) = \frac{b_0\left(1 + \frac{b_1}{b_0}z^{-1} + z^{-2}\right)}{1 + a_0 z^{-1} + a_1 z^{-2}} \tag{5}$$

where

a_0 , a_1, b_0, b_1 are the filter coefficients.

2.3.2. Digital comb filter

Different type of TEX-C biomedical sensor is expected to have different level of sensitivity toward the PLI and its harmonics. A comb filter was explored for this research because it has the advantage to suppress both the PLI fundamental frequency and its harmonics [43,44] The digital comb filter is designed based on the window method. The LabVIEW DFD IIR Comb Design VI by f_0 and BW is selected because the known targeted center frequency is 50 Hz. To achieve a fast roll-off with a sharp filter notch, 0.02 Hz of bandwidth at −50 dB is selected. Based on this frequency response characteristic, the corresponding filter coefficients are generated. The configuration parameters of the IIR digital comb filter are presented in Table 3. The comb filter implemented in this research, Notch Type I, has a transfer function as shown in equation (6). The frequency response and phase response graphs of the 50 Hz digital comb filter are presented in Fig. 4.

$$H(z) = \frac{b(1 - z^{-N})}{1 - az^{-N}} \tag{6}$$

where

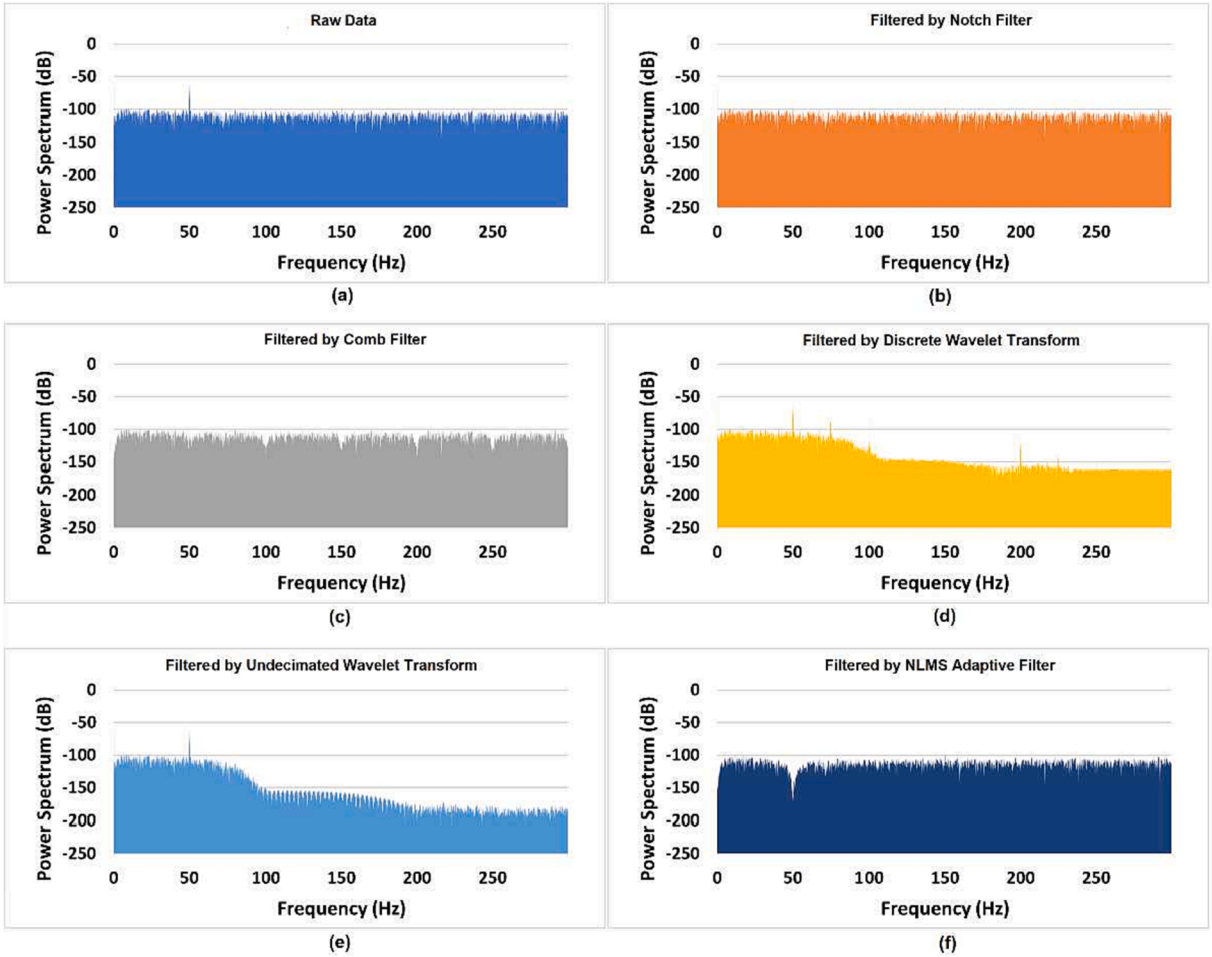

Fig. 10. Spectrum analysis of baseline data recorded by polyester TEX-C biomedical sensor.

a, b are the filter coefficients.

2.3.3. Wavelet denoise

Wavelet denoise is a technique that utilizes wavelet transformation to concentrate signal features into a few large-magnitude wavelet coefficients, while the low-magnitude wavelet coefficients are typically noise that can be suppressed or removed without affecting the overall signal quality [45–47]. Discrete wavelet transform (DWT) and undecimated wavelet transform (UWT) were implemented using LabVIEW Wavelet Denoise Express VI. The DWT downsampling the coefficients at each decomposition level while the UWT does not incorporate downsampling in the operation. The configuration parameters for both DWT and UWT are presented in Table 4 and Table 5. An orthogonal wavelet, Daubechies (db14) is selected because it is suitable for signal denoise application. The thresholding rule is set to "universal" which means that the threshold is equal to $sqrt(2 \times log(L_s))$, where L_s is the data length.

2.3.4. Adaptive filter

An adaptive filter is considered for this research as it has the advantage of dynamically adjusting the filter coefficient based on the inputs [48–50]. A finite impulse response (FIR) NLMS adaptive filter was implemented in this design. An NLMS adaptive filter is chosen over the least mean squares (LMS) adaptive filter because it has a better noise reduction capability and a faster convergence speed. Fig. 5 shows the block diagram of the NLMS adaptive filter. x(n) is the reference signal input to the adaptive filter. In this research, x(n) is the noise floor data collected simultaneously from the left-hand elbow of the subject which always remains at rest. The noise floor is a summation of random noises, 50 Hz PLI and its harmonics. d(n) is the EMG burst signals that are measured using the TEX-C biomedical sensor. y(n) is the output of the adaptive filter. e(n) is the filtered EMG burst signals calculated from the difference between the d(n) and y(n). The configuration parameters of the NLMS adaptive filter are presented in Table 6.

2.4. Experimental setup

Each TEX-C biomedical sensor was tested on two healthy subjects aged between 20 and 30 years old. This study was performed under relevant guidelines and regulations, and the protocol was approved by the Research Ethics Committee (REC) of Universiti Kebangsaan Malaysia. Informed consent was obtained from all the subjects.

This experiment was conducted in an electronic laboratory with an environmental temperature controlled at 25 degrees Celsius. The TEX-C biomedical sensors and the wet contact electrode were placed close to the subjects' bicep brachii to capture the EMG burst signals. Three types of data were collected during this experiment to be analyzed. The first type of data, also known as baseline characterization data, is measured when the subject's bicep brachii is in a relaxed and idle state. This data shows the power spectrum of the TEX-C biomedical sensors' initial noise floor and PLI amplitude. The power spectrum was plotted using LabVIEW FFT Power Spectrum and PSD for 1 Chan VI which performs a Fast Fourier Transform (FFT) on single channel data. The averaging mode selected is RMS averaging with a weighting mode set to linear to allow the averaging process to run 10 cycles. In general, the noise floor is expected to be a set of random data. Therefore, the Hanning window was applied in this process because it can preserve the frequency resolution

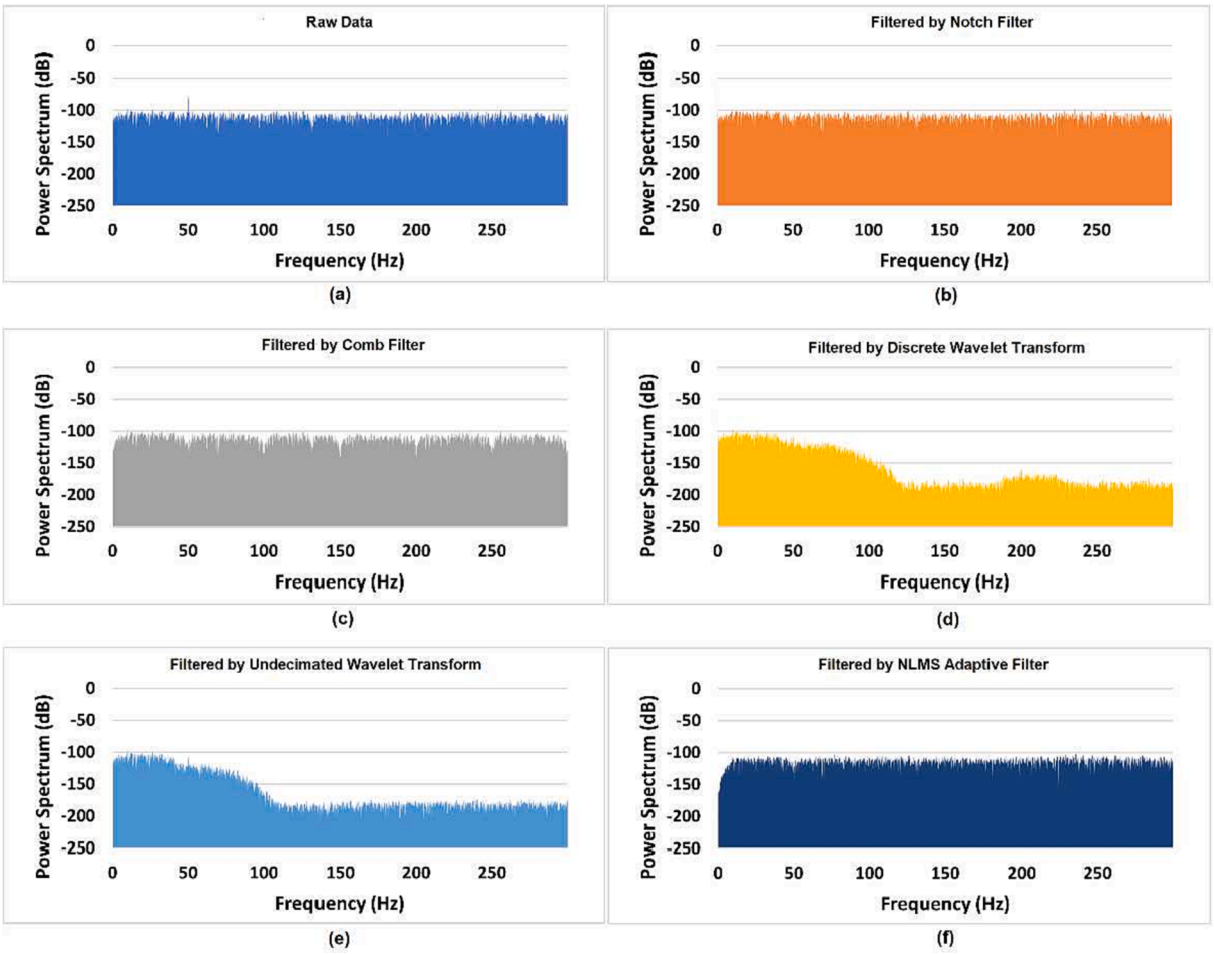

Fig. 11. Spectrum analysis of baseline data recorded by PVC-textile TEX-C biomedical sensor.

and amplitude accuracy of the resultant data.

The second type of data is known as dynamic muscle contraction data. This experiment started with the subject's forearm at rest on the table. Then, the subject is required to flex the forearm and arm to an angle of 45 degrees while remaining contracting the biceps brachii for one second. Next, the forearm will move back to the original position and remains at rest for 1 s. This activity is repeated three times within ten seconds. This data is a summation of the noise floor, PLI, and EMG burst signals captured by the TEX-C biomedical sensors.

The third type of data, also known as correlation analysis data, is measured when the subject contracted the bicep brachii for one second. During the one-second muscle contraction, the EMG burst signal is measured simultaneously by the TEX-C biomedical sensor and conventional wet contact electrode for direct performance comparison. All the data were processed using five types of digital filters and the results were compared and analyzed. The correlation coefficient (R) is calculated using equation (7).

$$R = \frac{\sum (x-\bar{x})(y-\bar{y})}{\sqrt{\sum (x-\bar{x})^2 \sum (y-\bar{y})^2}} \tag{7}$$

3. Results and discussion

3.1. Baseline characterization data

The baseline data of the six types of TEX-C biomedical sensors were recorded and post-processed. The spectrum analysis results of the raw data and digitally filtered data are presented in Figs. 6–11. The spectrum analysis allows a good understanding of the frequency components that exist in the baseline data. All the TEX-C biomedical sensors present a significant 50 Hz PLI. Nylon TEX-C biomedical sensor has the highest 50 Hz PLI power spectrum which was up to −43.4 dB, followed by polyester, rayon, and PVC-textile TEX-C biomedical sensor at −58.3 dB, −63.7 dB, and −76.7 dB respectively. Cotton and linen TEX-C biomedical sensors have similar amplitude at −73.4 dB and −73.8 dB respectively. As for the 50 Hz PLI harmonics, nylon, rayon, and polyester TEX-C biomedical sensor peak above −100 dB at 150 Hz.

The spectrum analysis results of raw data and digitally filtered in Figs. 6–11 provide a good insight into the 50 Hz PLI and harmonics suppression capability of all the digital filters and their response toward the input bandwidth. Notch filter, comb filter, and NLMS adaptive filer were able to suppress the 50 Hz PLI fundamental frequency effectively below −120 dB on all TEX-C biomedical sensors. However, only the comb filter can suppress all 50 Hz PLI harmonics below −120 dB on all TEX-C biomedical sensors. DWT and UWT have a nonlinear response across the input frequency bandwidth. The frequency range between 100 Hz and 300 Hz appeared to have a gain reduction on most of the TEX-C biomedical sensors. This effect is due to the use of a higher-order of Daubechies wavelet (dB14) to achieve a smoother wavelet. However, this characteristic will impact the accuracy of the EMG data which is expected to fall between 12 Hz and 300 Hz.

3.2. Dynamic muscle contraction data

This experiment evaluates the quality of raw EMG signals collected using six types of TEX-C biomedical sensors. Five different digital filters were implemented to observe their noise suppression capability in a

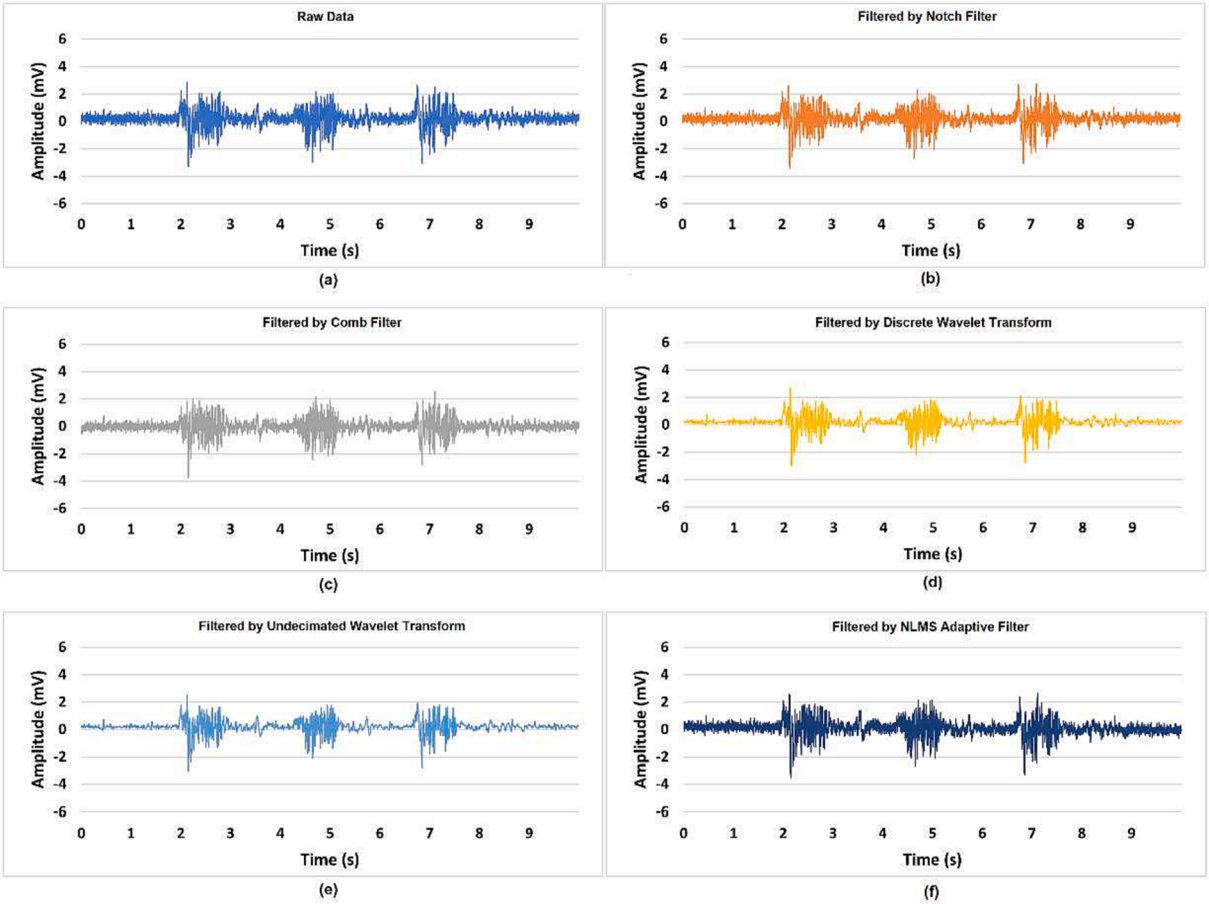

Fig. 12. Raw and post-processed EMG burst signals were recorded by a cotton TEX-C biomedical sensor.

real-life EMG signals measurement. All the raw data and digitally filtered data are presented in Figs. 12–17. The general noise floor of the TEX-C biomedical sensor is recorded when subjects' bicep brachii is idle. The EMG burst signal is recorded when the subjects contracted the bicep brachii.

The cotton and linen TEX-C biomedical sensors are capable of measuring three EMG burst signals clearly as shown in Figs. 12 (a) and 13 (a). Since these TEX-C biomedical sensors were having a low 50 Hz PLI power spectrum; therefore, the notch filter, comb filter, and NLMS adaptive filter did not significantly improve the overall data quality. Fig. 12(d), 12 (e), 13(d), and 13(e) indicate that the wavelet denoise filters produced a lower amplitude of noise floor compared to other filters. This is because the wavelet denoise filters have the characteristic of reducing the frequency gain between 100 Hz and 300 Hz to below 150 dB as shown in Section 3.1.

The raw EMG signals and filtered EMG signals measured by rayon, polyester, and PVC-textile TEX-C biomedical sensors are shown in Figs. 14, 16, and 17. The EMG data measured using these sensors recorded a higher amplitude of noise floor compared to cotton and linen TEX-C biomedical sensors. Polyester TEX-C biomedical sensor recorded the highest amplitude of noise floor among the three sensors which is $4.67mV_{p-p}$. Rayon and PVC-textile TEX-C biomedical sensor recorded similar amplitude of noise floor which are $3.37mV_{p-p}$ and $3.87mV_{p-p}$ respectively. The notch filter, comb filter, and NLMS adaptive filter all demonstrated good capability in suppressing the noise floor of all three biomedical sensors. The noise floor amplitude of the rayon, polyester, and PVC-textile TEX-C biomedical sensor was greatly suppressed below $2mV_{p-p}$. As for wavelet denoise filters, it was not able to specifically suppress the 50 Hz PLI fundamental frequency. When the raw data was significantly corrupted by the 50 Hz PLI, the wavelet denoise filters were not able to improve the signal-to-noise ratio as shown in Fig. 16(d) and 16(e).

Since the nylon TEX-C biomedical sensor recorded the highest 50 Hz PLI power spectrum among the six TEX-C biomedical sensors in Section 3.1, the noise floor amplitude of this TEX-C biomedical sensor was expected to be the highest as well. The raw EMG signals and filtered EMG signals measured by the nylon TEX-C biomedical sensor are presented in Fig. 15. The high noise floor of the nylon TEX-C biomedical sensor was out of the range of 6 mV to −6 mV and the three EMG burst signals were not visible. The notch filter, comb filter, and NLMS adaptive filter which were able to selectively suppress the 50 HZ PLI have greatly improved the signal quality. Fig. 15(b), 15(c), and 15(f) show the filter's output results respectively. Although the 50 Hz PLI had been suppressed, the filtered EMG burst signals were distorted. Fig. 15(d) and 15(e) show that wavelet denoise filters were not able to suppress the 50 Hz PLI. The filter output results remained the same as the raw data in Fig. 15(a).

3.3. Correlation analysis data

The performance of six TEX-C biomedical sensors was compared against the wet contact electrode (Ag-AgCl) because it is the gold standard in electrophysiological signals measurement. The correlation coefficients (R) of the raw EMG signals measured by six TEX-C biomedical sensors and a wet contact electrode set the baseline performance of the TEX-C biomedical sensors. The correlation coefficients (R) of the filtered EMG signals were generated as well to quantify their performance improvement or degradation against the baseline performance of each TEX-C biomedical sensor. The EMG signal measurement was repeated twice on each subject to ensure the reproducibility and reliability of the data. The average correlation coefficients of the two subjects are

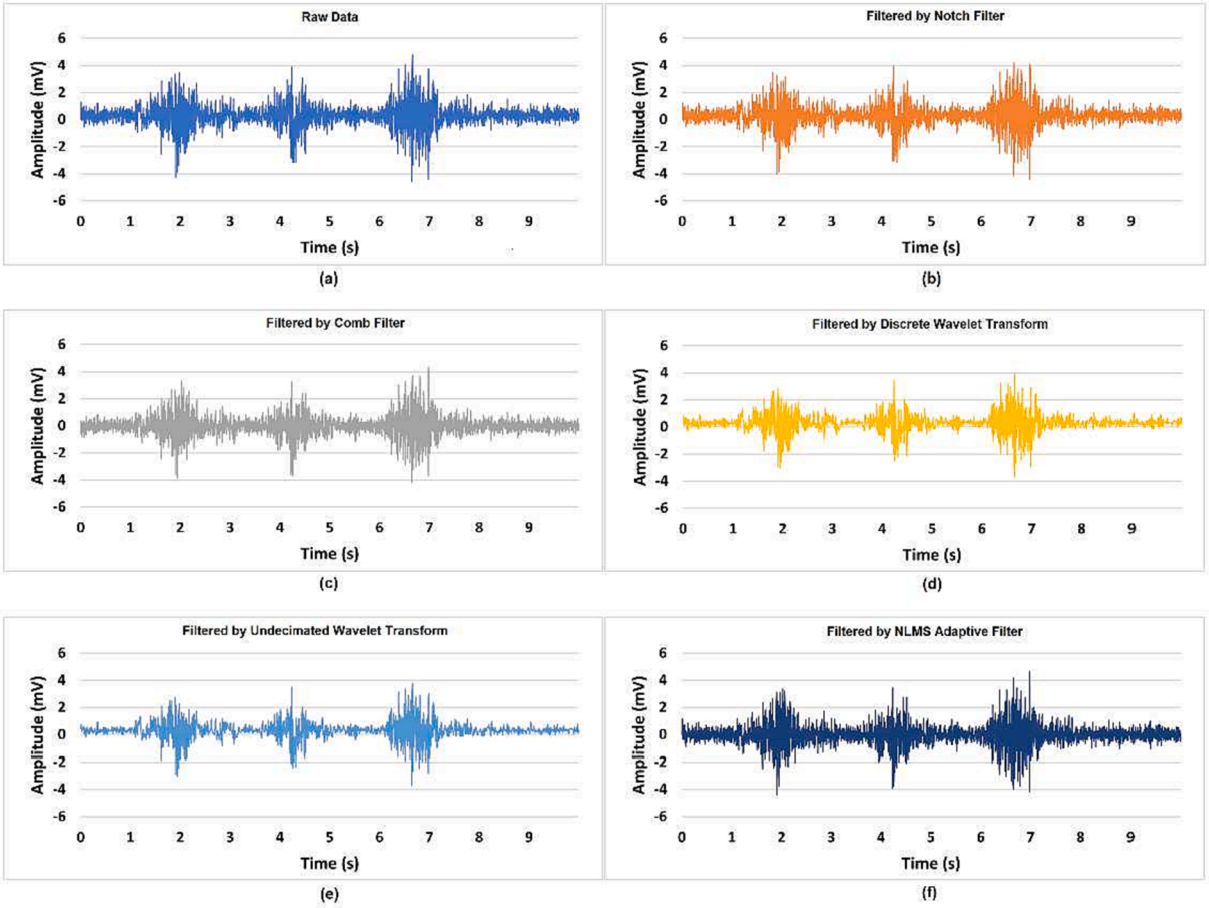

Fig. 13. Raw and post-processed EMG burst signals were recorded by a linen TEX-C biomedical sensor.

presented in Fig. 18 and Table 7.

EMG signals captured by rayon insulated TEX-C biomedical sensor and wet contact electrode achieved the highest correlation coefficient of 0.846 after post-processed by comb filter. Fig. 19 shows the improvement of correlation between raw data, comb-filtered data, and EMG signals measured by the wet contact electrode. The cotton, linen, and PVC-textile TEX-C biomedical sensors have higher skin-electrode capacitance compared with other textile materials; thus, they are less susceptible to the 50 Hz PLI. The correlation coefficient results show that the raw signals measured by cotton, linen, and PVC-textile TEX-C biomedical sensors versus the wet contact electrode have a high correlation coefficient above 0.73. Digital filters such as notch filter and comb filter only can offer slight improvement to the overall results. On the other hand, rayon, nylon, and polyester TEX-C biomedical sensor are more susceptible to 50 Hz PLI due to the relatively low skin-electrode capacitance. Notch filter, comb filter, and NLMS adaptive filter help to suppress the 50 Hz PLI in the signals and improved the signal-to-noise ratio. Therefore, the correlation coefficient of the EMG signals post-processed by these filters achieved significant improvement. The correlation coefficient of rayon TEX-C biomedical sensor improves from 0.665 to above 0.756 while the correlation coefficient of polyester TEX-C biomedical sensor improves from 0.437 to above 0.700. The correlation coefficient of nylon TEX-C biomedical sensor improves from no correlation, −0.007 to 0.454, 0.400, and 0.169 after post-processed by comb filter, notch filter, and NLMS adaptive filters respectively. DWT and UWT filters recorded a degradation of correlation coefficient values for almost all TEX-C biomedical sensors because the frequency components within the interested input bandwidth of 12 Hz–300 Hz are suppressed. Overall, the correlation coefficient (R) results are aligned with the observation in Section 3.2, dynamic muscle contraction data. Digital filters with the ability to specifically suppress 50 Hz PLI and harmonics will be able to improve the performance of all six TEX-C biomedical sensors.

3.4. *Digital filters performance comparison*

A real-life EMG signals measurements approach has been taken to evaluate the performance of six TEX-C biomedical sensors and five digital filters. The digital filters' characteristics and effectiveness in suppressing the 50 Hz PLI and harmonics are presented in Sections 3.1–3.3 as well. Table 8 provides a performance summary of the digital filters against the 50 Hz PLI and harmonics of six types of TEX-C biomedical sensors.

All digital filters only require a raw EMG data input to operate except for the NLMS adaptive filter which requires an additional noise floor reference data as an input to effectively cancel off the 50 Hz PLI. This requirement creates an additional hardware circuitry and analog-to-digital (ADC) input onboard to continuously collect the noise floor as reference data. Eventually, the TEX-C biomedical sensor becomes too bulky and inconvenient for system integration. Notch filter, comb filter, and NLMS adaptive filter all have good 50 Hz PLI suppression across the six TEX-C biomedical sensors, which are below −120 dB, −130 dB, and 140 dB respectively. NLMS adaptive filter has the highest 50 Hz PLI suppression capability. The comb filter is the only digital filter capable of suppressing the 50 Hz PLI harmonics and reducing the harmonics' power spectrum down below −130 dB. Wavelet denoise filters such as DWT and UWT will reduce the signal gain between 100 Hz and 300 Hz. This characteristic affects the overall signal quality within the interested input bandwidth from 12 Hz to 300 Hz. The last column of Table 8 summarized which digital filter can help the six TEX-C biomedical

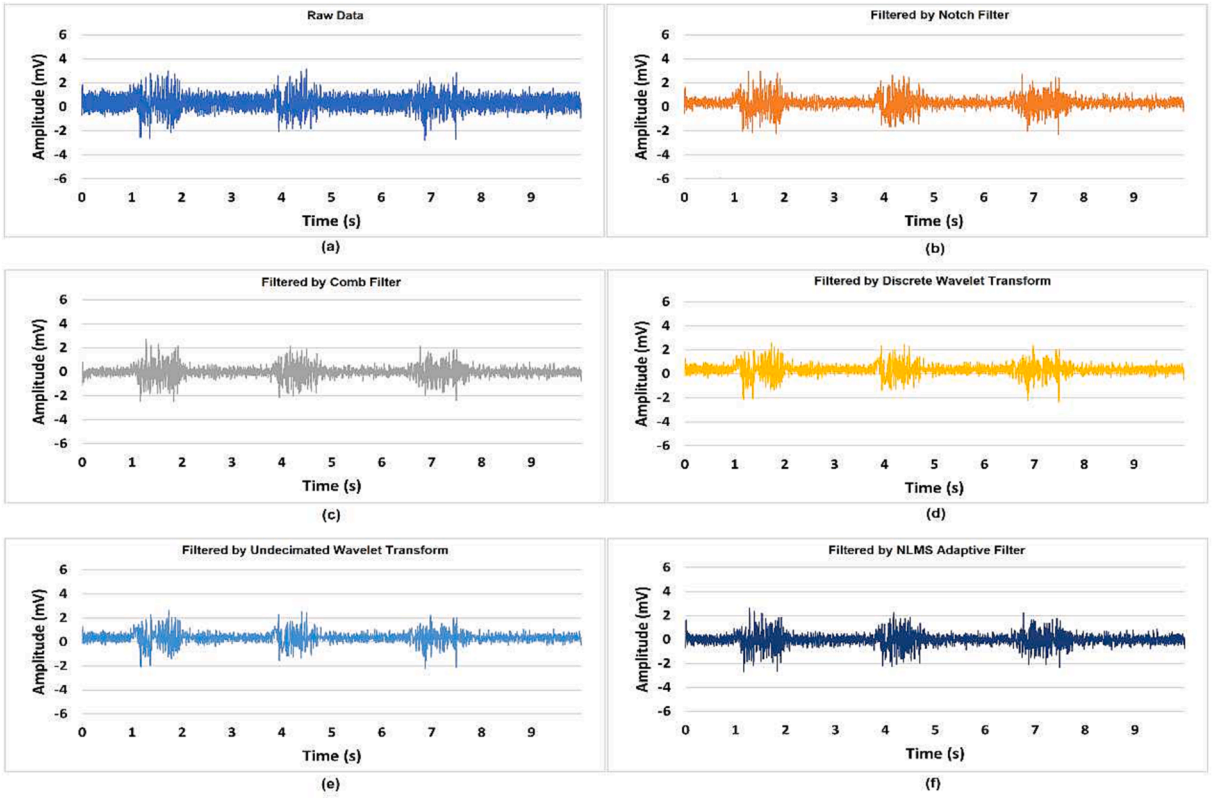

Fig. 14. Raw and post-processed EMG burst signals were recorded by a rayon TEX-C biomedical sensor.

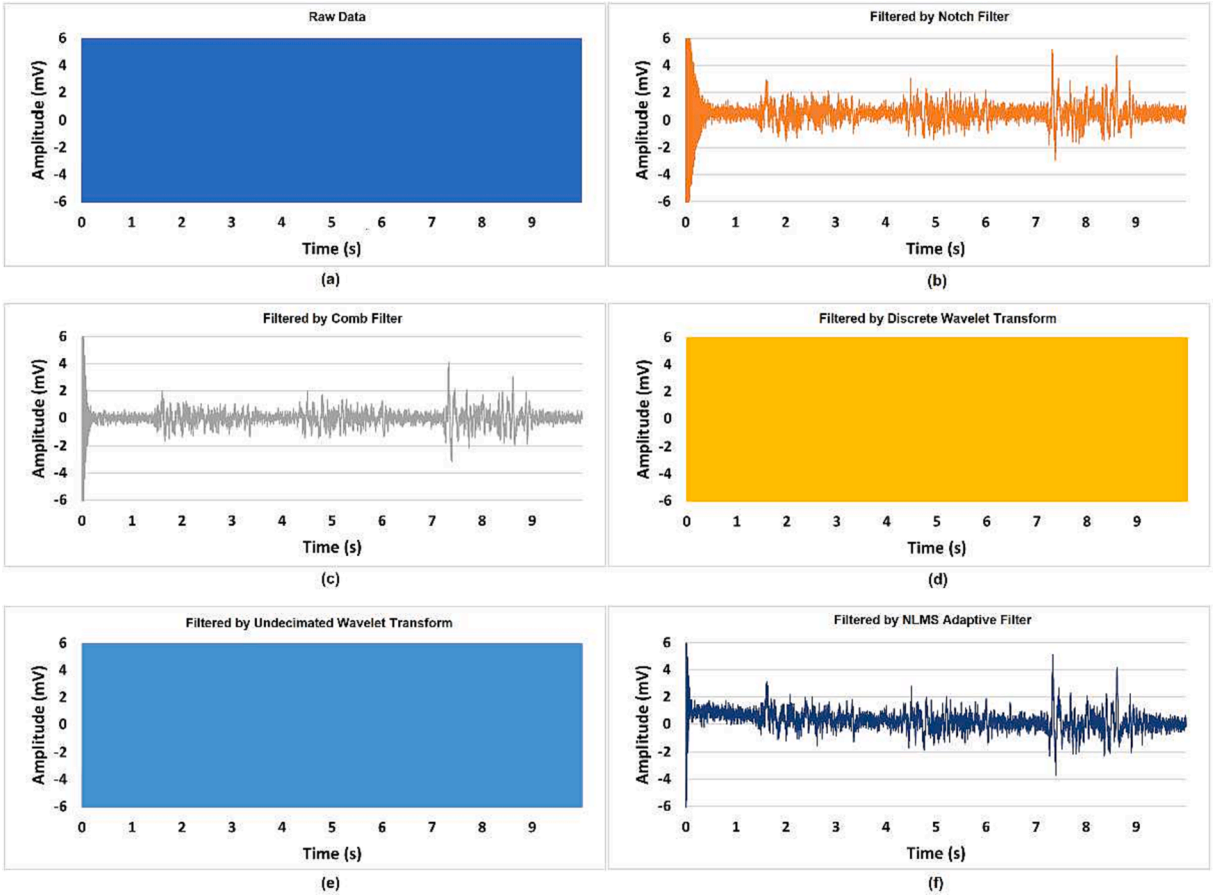

Fig. 15. Raw and post-processed EMG burst signals were recorded by a nylon TEX-C biomedical sensor.

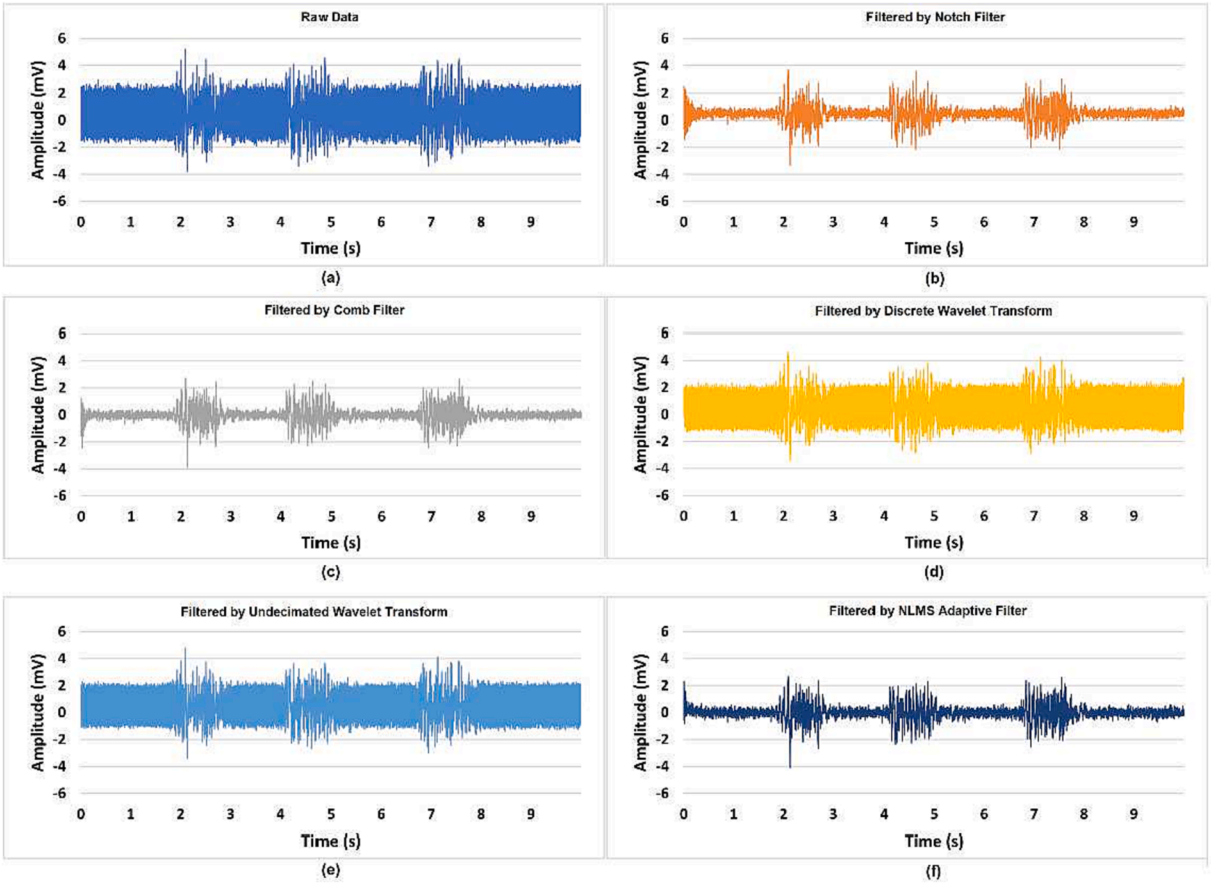

Fig. 16. Raw and post-processed EMG burst signals were recorded by a polyester TEX-C biomedical sensor.

sensors can achieve the highest improvement of correlation coefficient. Comb filter has helped linen, rayon, nylon, and polyester TEX-C biomedical sensors to achieve the highest correlation coefficient improvement. Cotton TEX-C biomedical sensor achieved the highest correlation coefficient improvement with UWT filter while PVC-textile TEX-C biomedical sensor achieved the highest correlation coefficient improvement with NLMS adaptive filter. With the implementation of comb filter in digital signal processing stage can improve the EMG signals quality to become identical to the signals measure by wet contact electrode, the existing gold standard.

The signal path of a capacitive EMG measurement system typically consists of analog and digital domains as shown in Fig. 1. A TEX-C biomedical sensor operates in the analog domain while the data acquisition unit converts the data from the analog to the digital domain. An analog bandpass filter is generally required to characterize the input bandwidth and act as an anti-aliasing filter before converting the signal to the digital domain. For additional filters that are being used for feature extraction or noise filtering such as PLI suppression, the system designer has the option to implement it in either analog or digital domain. In general, a digital filter has a start-up latency compared to an analog filter. Besides that, the operation speed of the digital filter has a dependency on the ADC sampling frequency. Referring to Fig. 15 and Fig. 18, if the PLI has saturated the analog frontend, implementing the backend digital filter is not able to improve the signal quality and becomes similar to the wet contact electrode. A differential amplifier can be implemented at the analog frontend to reduce the common-mode noise or an additional analog filter is required before conversion from the analog domain to the digital domain. On the other hand, implementing PLI filter in the analog domain will increase the size and weight of a wearable sensor because additional components and PCB area were required. Typical notch filter architectures such as Twin-T topology or Fliege topology required high-precision value matching of passive components to achieve accurate center frequency and high Q-factor. The textile-based capacitive ECG acquisition system designed by Li et al. suppresses the PLI using an analog filter. A twin-T notch filter and additional three operational amplifiers were added to the frontend circuitry while the 50 Hz PLI suppression is only down to −8 dB with a relatively low Q-factor [21]. Gao et al. implemented an analog twin-T notch filter for a flexible capacitive ECG electrode as well [51]. The notch filter can achieve good 60 Hz PLI suppression but the target ECG bandwidth between 0.3 Hz and 100 Hz has been compromised. The signal gain starts to attenuate around 40 Hz while the signal gain between 61 Hz and 100 Hz is 30 % lower than the input signal. It is mainly due to the effect of a low Q-factor. In comparison with the digital notch filter presented in Section 2.3.1, frequency response with high Q-factor of 20 and sharp attenuation down to −14 dB were able to achieve. The chair-based ECG sensor developed by Hou et al. has a combination of 50 Hz analog and digital notch filters. Although the analog notch filter has been implemented, additional digital notch filter is still required for eliminating the PLI [22]. To miniaturize the hardware and optimize the performance, this paper proposed to implement PLI in the digital domain. A digital filter has advantages of higher flexibility to be redesigned and reconfigured without incurring significant development costs and time compared to an analog filter. High Q-factor and passband gain can be achieved with digital filter as shown in Fig. 3 and Fig. 4. Based on the experimental results in this paper, a digital comb filter has enabled the TEX-C biomedical sensor to be insulated by six types of textile material while yielding a high correlation of EMG signals measured by the conventional wet contact electrode. Digital comb filter has greatly improved the versatility of the generic TEX-C biomedical sensor to be insulated by different kinds of textile materials.

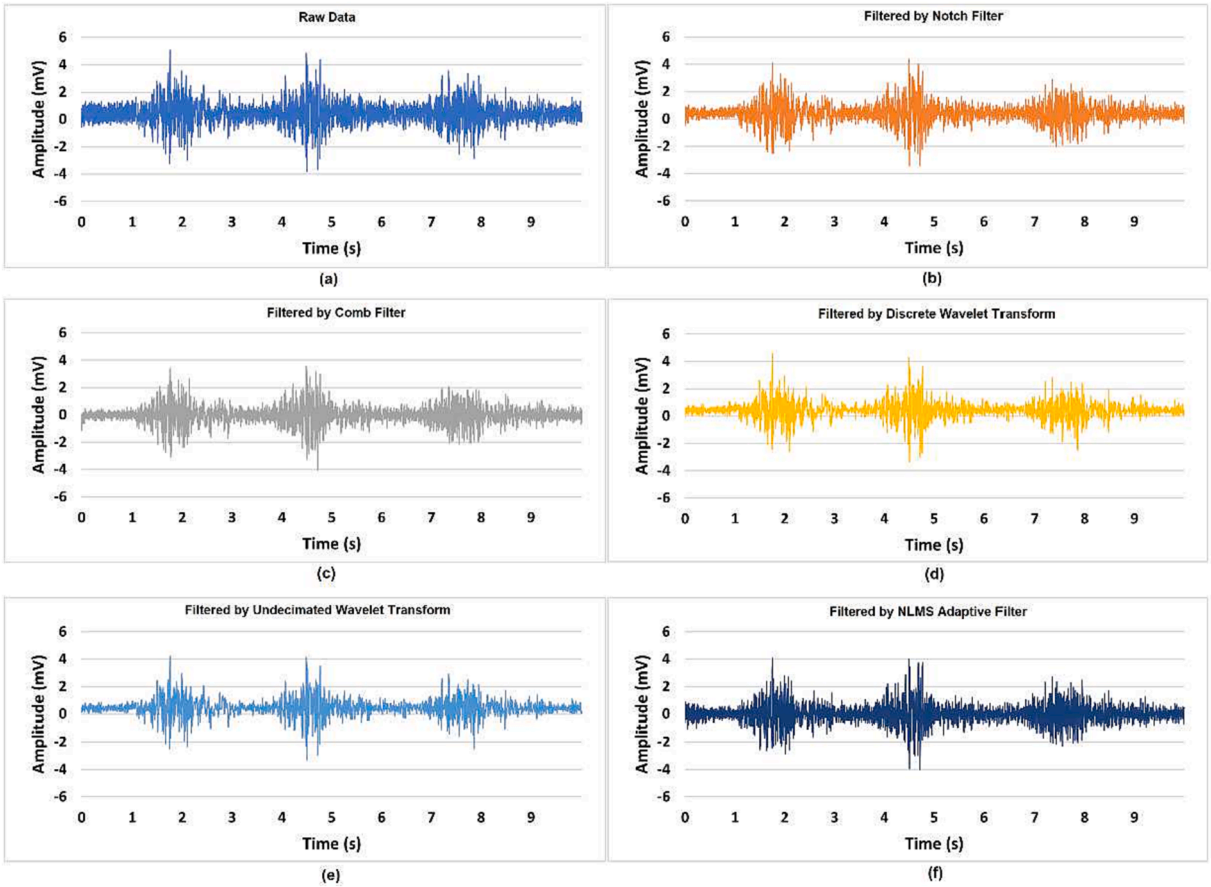

Fig. 17. Raw and post-processed EMG burst signals were recorded by a PVC-textile TEX-C biomedical sensor.

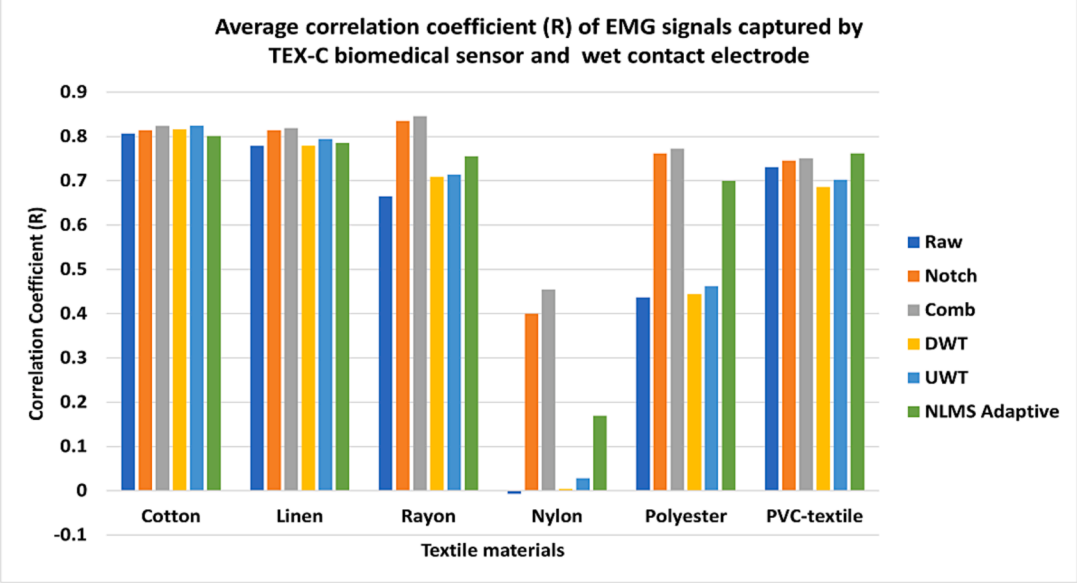

Fig. 18. An average correlation coefficient (R) of EMG signals captured by TEX-C biomedical sensor and wet contact electrode.

4. Conclusions

The goal of this paper is to propose a simplified system architecture that allows generic hardware of the TEX-C biomedical sensor to yield a quality signal measurement despite significant PLI contributed by different types of textile insulators. The unique amplitudes and characteristics of the power spectrum of 50 Hz PLI and harmonics of six types of TEX-C biomedical sensors were first presented in this paper. Theoretical analysis is in line with experimental analysis which has proven that 50 Hz PLI and harmonics are the dominant interference of a TEX-C biosensor. The amplitude of the 50 Hz PLI is proportional to the skin-electrode capacitance value which is impacted by the physical properties of each textile material such as thickness, porosity, and relative permittivity. This research proposed that a generic and versatile TEX-C

Table 7
Summary of the correlation coefficient and values changes between raw data and post-processed data.

Insulating material	Correlation coefficient of raw data	Digital Filters	Correlation coefficient of filtered data	Changes in correlation coefficient value between raw data and filtered data
Cotton	0.807	Notch	0.814	0.007
		Comb	0.823	0.016
		DWT	0.817	0.010
		UWT	0.825	0.018
		NLMS Adaptive	0.801	−0.006
Linen	0.779	Notch	0.814	0.035
		Comb	0.819	0.040
		DWT	0.779	0.000
		UWT	0.794	0.015
		NLMS Adaptive	0.785	0.006
Rayon	0.665	Notch	0.835	0.170
		Comb	0.846	0.181
		DWT	0.709	0.044
		UWT	0.714	0.049
		NLMS Adaptive	0.756	0.091
Nylon	−0.007	Notch	0.400	0.407
		Comb	0.454	0.461
		DWT	0.004	0.010
		UWT	0.028	0.034
		NLMS Adaptive	0.169	0.176
Polyester	0.437	Notch	0.762	0.325
		Comb	0.772	0.336
		DWT	0.444	0.007
		UWT	0.462	0.025
		NLMS Adaptive	0.700	0.263
PVC-textile	0.731	Notch	0.746	0.015
		Comb	0.751	0.020
		DWT	0.686	−0.044
		UWT	0.702	−0.029
		NLMS Adaptive	0.762	0.031

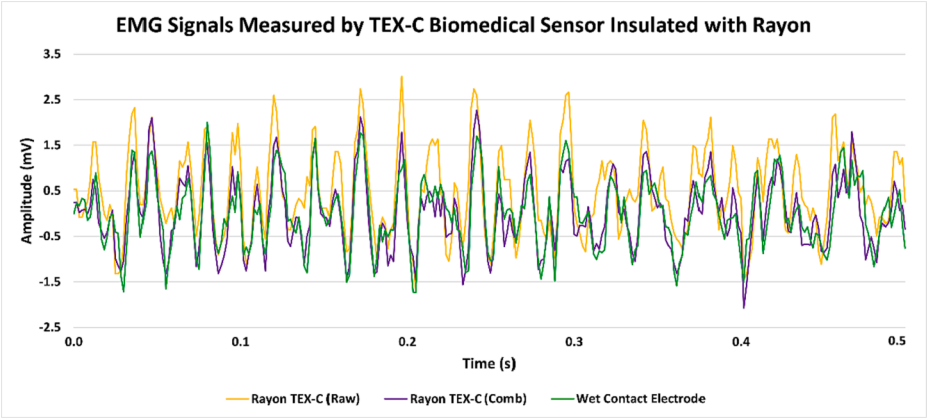

Fig. 19. Raw and post-processed EMG signals measured by TEX-C biomedical sensor and wet contact electrode.

Table 8
Performance summary of five digital filters across six TEX-C biomedical sensors.

Filters	Input data requirement	50 Hz PLI suppression	PLI harmonics suppression	Affect input bandwidth	Textile with highest (R) improvement
Notch	Raw data	below −120 dB	–	No	–
Comb	Raw data	below −130 dB	below −130 dB	No	Linen (+0.040), Rayon (+0.181), Nylon (+0.461), Polyester (+0.336)
DWT	Raw data	–	–	Yes	–
UWT	Raw data	–	–	Yes	Cotton (+0.016)
NLMS adaptive	Raw data & Noise floor ref. data	below −140 dB	–	No	PVC-Textile (+0.031)

biomedical sensor can be realized with the implementation of a 50 Hz comb filter in the digital signal processing stage to actively suppress the 50 Hz PLI and harmonics below −130 dB. With this additional comb filter, significant correlation improvements of the EMG signals measured by the wet contact electrode and TEX-C biomedical sensor insulated by cotton (0.823), linen (0.819), rayon (0.846), nylon (0.454), polyester (0.772), and PVC-textile (0.751) were achieved. A digital comb filter also has the advantages of being flexible, reconfigurable, low cost, and

having no additional hardware components on the existing TEX-C biomedical sensor in comparison with an analog filter. This simplified architecture enabled the generic TEX-C biomedical sensor compatible with different textile insulators. This research outcome opens ample opportunities to integrate a capacitive biomedical sensor in a variety of clothing to advance smart garments, sport science, human–machine interface, and remote healthcare applications.

5. Informed consent statement

Written informed consent was obtained from all subjects participating in this study.

Funding information

This research is financially supported by Universiti Kebangsaan Malaysia (UKM), Grant No. GUP-2021-019, UKM-TR-011, and DIP-2020-004 and Qatar National Research Foundation (QNRF) grant no. NPRP12s-0227-190164 and International Research Collaboration Co-Fund (IRCC) grant: IRCC-2021-001. Open Access publication of this article is supported by Qatar National Library. The statements made herein are solely the responsibility of the authors.

CRediT authorship contribution statement

Charn Loong Ng: Conceptualization, Methodology, Data curation, Formal analysis, Writing – original draft. **Mamun Bin Ibne Reaz:** Methodology, Resources, Supervision. **Sawal Hamid Bin Md Ali:** Resources, Writing – review & editing. **Maria Liz Crespo:** Formal analysis, Supervision. **Andres Cicuttin:** Data curation, Formal analysis. **Muhammad Enamul Hoque Chowdhury:** Resources, Supervision. **Serkan Kiranyaz:** Resources, Writing – review & editing. **Noorfazila Binti Kamal:** Supervision, Writing – review & editing.

Declaration of Competing Interest

The authors declare that they have no known competing financial interests or personal relationships that could have appeared to influence the work reported in this paper.

Data availability

The authors do not have permission to share data.

Acknowledgments

This work is partially supported by the ICTP through the Affiliated Centres Programme and STEP program of International Centre for Theoretical Physics (ICTP), Italy are gratefully acknowledged.

References

[1] J. Heikenfeld, et al., Wearable sensors: modalities, challenges, and prospects, Lab Chip 18 (2) (2018), https://doi.org/10.1039/c7lc00914c.
[2] J. Kim, A.S. Campbell, B.E.F. de Ávila, J. Wang, Wearable biosensors for healthcare monitoring, Nat. Biotechnol. 37 (4) (2019), https://doi.org/10.1038/s41587-019-0045-y.
[3] A. Sharma, M. Badea, S. Tiwari, J.L. Marty, Wearable biosensors: an alternative and practical approach in healthcare and disease monitoring, Molecules 26 (3) (2021), https://doi.org/10.3390/molecules26030748.
[4] S.C. Mukhopadhyay, Wearable sensors for human activity monitoring: a review, IEEE Sens. J. 15 (3) (2015), https://doi.org/10.1109/JSEN.2014.2370945.
[5] S. Pillai, A. Upadhyay, D. Sayson, B.H. Nguyen, S.D. Tran, Advances in medical wearable biosensors: design, fabrication and materials strategies in healthcare monitoring, Molecules 27(1) (2022), doi: 10.3390/molecules27010165.
[6] C.W. Mundt, et al., A multiparameter wearable physiologic monitoring system for space and terrestrial applications, IEEE Trans. Inf. Technol. Biomed. 9 (3) (2005), https://doi.org/10.1109/TITB.2005.854509.
[7] R. Paradiso, G. Loriga, N. Taccini, A wearable health care system based on knitted integrated sensors, IEEE Trans. Inf. Technol. Biomed. 9 (3) (2005), https://doi.org/10.1109/TITB.2005.854512.
[8] M. di Rienzo, F. Rizzo, G. Parati, G. Brambilla, M. Ferratini, P. Castiglioni, MagIC system: a new textile-based wearable device for biological signal monitoring. Applicability in daily life and clinical setting, in: Annual International Conference of the IEEE Engineering in Medicine and Biology - Proceedings, 2005, Vol. 7, doi: 10.1109/iembs.2005.1616161.
[9] K.J. Heilman, S.W. Porges, Accuracy of the LifeShirt® (Vivometrics) in the detection of cardiac rhythms, Biol. Psychol. 75 (3) (2007), https://doi.org/10.1016/j.biopsycho.2007.04.001.
[10] I. Poitras, M. Bielmann, A. Campeau-Lecours, C. Mercier, L.J. Bouyer, J.S. Roy, Validity of wearable sensors at the shoulder joint: combining wireless electromyography sensors and inertial measurement units to perform physical workplace assessments, Sensors (Switzerland) 19 (8) (2019), https://doi.org/10.3390/s19081885.
[11] S. Pizzolato, L. Tagliapietra, M. Cognolato, M. Reggiani, H. Müller, M. Atzori, Comparison of six electromyography acquisition setups on hand movement classification tasks, PLoS ONE 12 (10) (2017), https://doi.org/10.1371/journal.pone.0186132.
[12] Y. Choi, J. Lee, Effect of peroneus longus muscle release on abductor hallucis muscle activity and medial longitudinal arch before toe-tap exercise in participants with flexible pes planus, Healthcare (Switzerland) 10 (1) (2022), https://doi.org/10.3390/healthcare10010044.
[13] H. Pasini Neto, et al., Effect of posture-control insoles on function in children with cerebral palsy: randomized controlled clinical trial, BMC Musculoskelet. Disord. 13 (2012), https://doi.org/10.1186/1471-2474-13-193.
[14] T. Bednár, B. Babušiak, Measurement of capacitive coupled ECG from the car seat, Transp. Res. Proc. (2019), https://doi.org/10.1016/j.trpro.2019.07.175.
[15] Y.M. Chi, T.P. Jung, G. Cauwenberghs, Dry-contact and noncontact biopotential electrodes: methodological review, IEEE Rev. Biomed. Eng. 3 (2010) 106–119, https://doi.org/10.1109/RBME.2010.2084078.
[16] C.L. Ng, M.B.I. Reaz, Evolution of a capacitive electromyography contactless biosensor: design and modelling techniques, Measur.: J. Int. Measur. Confederat. (2019), https://doi.org/10.1016/j.measurement.2019.05.031.
[17] Ko Keun Kim, Yong Kyu Lim, Kwang Suk Park, Common mode noise cancellation for electrically non-contact ECG measurement system on a chair, in: 2005 IEEE Engineering in Medicine and Biology 27th Annual Conference, 2005, pp. 5881–5883, doi: 10.1109/IEMBS.2005.1615828.
[18] Y.G. Lim, G.S. Chung, K.S. Park, Capacitive driven-right-leg grounding in indirect-contact ECG measurement, in 2010 Annual International Conference of the IEEE Engineering in Medicine and Biology Society, EMBC'10, 2010, doi: 10.1109/IEMBS.2010.5626424.
[19] C. Levkov, G. Mihov, R. Ivanov, I. Daskalov, I. Christov, I. Dotsinsky, Removal of power-line interference from the ECG: a review of the subtraction procedure, Biomed. Eng. Online (2005), https://doi.org/10.1186/1475-925X-4-50.
[20] A. Ueno, Y. Akabane, T. Kato, H. Hoshino, S. Kataoka, Y. Ishiyama, Capacitive sensing of electrocardiographic potential through cloth from the dorsal surface of the body in a supine position: a preliminary study, I.E.E.E. Trans. Biomed. Eng. 54 (4) (2007) 759–766, https://doi.org/10.1109/TBME.2006.889201.
[21] H. Li, et al., Textile-based ECG acquisition system with capacitively coupled electrodes, Trans. Inst. Meas. Control (2017), https://doi.org/10.1177/0142331215600254.
[22] Z. Hou, J. Xiang, Y. Dong, X. Xue, H. Xiong, B. Yang, Capturing electrocardiogram signals from chairs by multiple capacitively coupled unipolar electrodes, Sensors (Switzerland) (2018), https://doi.org/10.3390/s18092835.
[23] S. Pfeiffer, et al., Motion-induced imbalance of contact impedance in ECG capture: comparison of electrode materials in capacitive coupling, Proc. IEEE Sensors (2019), https://doi.org/10.1109/SENSORS43011.2019.8956609.
[24] A. Takano, H. Ishigami, A. Ueno, Non-contact measurements of electrocardiogram and cough-associated electromyogram from the neck using in-pillow common cloth electrodes: a proof-of-concept study, Sensors (Switzerland) (2021), https://doi.org/10.3390/s21030812.
[25] C.L. Ng, M.B.I. Reaz, Characterization of textile-insulated capacitive biosensors, Sensors (Switzerland) 17 (3) (2017), https://doi.org/10.3390/s17030574.
[26] D.T. Mewett, H. Nazeran, K.J. Reynolds, Removing power line noise from recorded EMG, in: Annual Reports of the Research Reactor Institute, Kyoto University, 2001, doi: 10.1109/iembs.2001.1017205.
[27] H. Li, J. Zhang, L. Wang, A fully integrated continuous-time 50-Hz notch filter with center frequency tunability, in: Proceedings of the Annual International Conference of the IEEE Engineering in Medicine and Biology Society, EMBS, 2011, doi: 10.1109/IEMBS.2011.6090593.
[28] H. Posada-Quintero, R. Rood, K. Burnham, J. Pennace, K. Chon, Assessment of carbon/salt/adhesive electrodes for surface electromyography measurements, IEEE J. Transl. Eng. Health Med. (2016), https://doi.org/10.1109/JTEHM.2016.2567420.
[29] M.K. Hazrati, H.M. Husin, U.G. Hofmann, Wireless brain signal recordings based on capacitive electrodes, in: 2013 IEEE 8th International Symposium on Intelligent Signal Processing, WISP 2013 - Proceedings, 2013, pp. 8–13, doi: 10.1109/WISP.2013.6657474.
[30] C.L. Ng, M.B.I. Reaz, M.E.H. Chowdhury, A low noise capacitive electromyography monitoring system for remote healthcare applications, IEEE Sens. J. (2020), https://doi.org/10.1109/JSEN.2019.2957068.
[31] L. Shaw, S. Bagha, Online EMG signal analysis for diagnosis of neuromuscular diseases by using PCA and PNN, Int. J. Eng. Sci. (2012).

[32] R. Salvado, C. Loss, R. Gon, P. Pinho, Textile materials for the design of wearable antennas: a survey, Sensors (Switzerland) (2012), https://doi.org/10.3390/s121115841.
[33] P.J. Žilinskas, T. Lozovski, V. Jankauskas, J. JurkŠus, Electrostatic properties and characterization of textile materials affected by ion flux, Medziagotyra 19(1) (2013), doi: 10.5755/j01.ms.19.1.3828.
[34] C.H. Park, Y.K. Kang, S.S. Im, Biodegradability of cellulose fabrics, J. Appl. Polym. Sci. 94 (1) (2004) 248–253, https://doi.org/10.1002/app.20879.
[35] G. Buschle-Diller, S.H. Zeronian, N. Pan, M.Y. Yoon, Enzymatic hydrolysis of cotton, linen, ramie, and viscose rayon fabrics, Text. Res. J. 64 (5) (1994) 270–279, https://doi.org/10.1177/004051759406400504.
[36] Ţ.D. Daniel, M.N. Ungureanu, R. Strungaru, Cancelling harmonic power line interference in biopotentials, in: Compendium of New Techniques in Harmonic Analysis, 2018, https://doi.org/10.5772/intechopen.74579.
[37] T. Roland, K. Wimberger, S. Amsuess, M.F. Russold, W. Baumgartner, An insulated flexible sensor for stable electromyography detection: application to prosthesis control, Sensors 19(4) (2019), doi: 10.3390/s19040961.
[38] C.L. Ng, M. Bin Ibne Reaz, Impact of skin-electrode capacitance on the performance of CEMG biosensor, IEEE Sens. J. 17 (9) (2017) 2636–2637, https://doi.org/10.1109/JSEN.2017.2675707.
[39] J. Piskorowski, Time-efficient removal of power-line noise from EMG signals using IIR notch filters with non-zero initial conditions, Biocybern. Biomed. Eng. 33 (3) (2013) 171–178, https://doi.org/10.1016/j.bbe.2013.07.006.
[40] Y.S. Chen, P.Y. Lin, Y. der Lin, A novel PLI suppression method in ECG by notch filtering with a modulation-based detection and frequency estimation scheme, Biomed. Signal Process. Control (2020), https://doi.org/10.1016/j.bspc.2020.102150.
[41] C.L. Ng, M.B.I. Reaz, M.L. Crespo, A. Cicuttin, M.E.H. Chowdhury, Characterization of capacitive electromyography biomedical sensor insulated with porous medical bandages, Sci. Rep. (2020), https://doi.org/10.1038/s41598-020-71709-0.
[42] A. Ben Slimane, A. Zaid, Real-Time fast fourier transform-based notch filter for single-frequency noise cancellation: application to electrocardiogram signal denoising," J. Med. Signals Sens. (2021), doi: 10.4103/jmss.JMSS-3-20.
[43] R.K. Ranjan, C.K. Choubey, B.C. Nagar, S.K. Paul, Comb filter for elimination of unwanted power line interference in biomedical signal, J. Circuits Syst. Comput. (2016), https://doi.org/10.1142/S0218126616500523.
[44] S.K. Paul, C.K. Choubey, G. Tiwari, Low power analog comb filter for biomedical applications, Analog Integr. Circ. Sig. Process (2018), https://doi.org/10.1007/s10470-018-1329-8.
[45] J.J. Galiana-Merino, D. Ruiz-Fernandez, J.J. Martinez-Espla, Power line interference filtering on surface electromyography based on the stationary wavelet packet transform, Comput. Methods Programs Biomed. (2013), https://doi.org/10.1016/j.cmpb.2013.04.022.
[46] R.D. Mali, M.S. Khadtare, U.L. Bombale, Removal of 50Hz PLI using discrete wavelet transform for quality diagnosis of biomedical ECG signal, Int. J. Comput. Appl. (2011), https://doi.org/10.5120/2902-3805.
[47] L. El Bouny, M. Khalil, A. Adib, Removal of 50Hz PLI from ECG signal using undecimated wavelet transform, in: Proceedings - 2017 International Conference on Wireless Networks and Mobile Communications 2017, 2017, https://doi.org/10.1109/WINCOM.2017.8238206.
[48] M. Tomasini, S. Benatti, B. Milosevic, E. Farella, L. Benini, Power line interference removal for high-quality continuous biosignal monitoring with low-power wearable devices, IEEE Sens. J. (2016), https://doi.org/10.1109/JSEN.2016.2536363.
[49] A.K. Ziarani, A. Konrad, A nonlinear adaptive method of elimination of power line interference in ECG signals, IEEE Trans. Biomed. Eng. (2002), https://doi.org/10.1109/TBME.2002.1001968.
[50] J. Lin, X. Sun, J. Wu, S.C. Chan, W. Xu, Removal of power line interference in EEG signals with spike noise based on robust adaptive filter, in: IEEE Region 10 Annual International Conference, Proceedings/TENCON, 2017, doi: 10.1109/TENCON.2016.7848531.
[51] Y. Gao, et al., Heart Monitor Using Flexible Capacitive ECG Electrodes, IEEE Trans. Instrum. Meas. 69 (7) (2020) 4314–4323, https://doi.org/10.1109/TIM.2019.2949320.